Preclinical testing of RRx-001 in mouse models of experimental endometriosis reveals promising therapeutic impacts

Iona McIntyre[1, 2], Vadim Vasilyev[1], Chiara Lia Perrone[1], Priya Dhami[1, 2], Kavita Panir[1, 2], Matthew Rosser[1, 2], Erin Greaves[1, 2]

1. Division of Biomedical Sciences, Warwick Medical School, University of Warwick, Coventry, United Kingdom (UK)
2. Centre for Early Life, University of Warwick, Coventry, UK

Corresponding author: Dr Erin Greaves

Email: Erin.Greaves@Warwick.ac.uk

Tel: 024 7696 8640

Key words: Endometriosis, therapeutic, macrophage

Abstract

Endometriosis is a chronic inflammatory condition characterised by the presence of ectopic endometrial-like tissue (lesions), associated reduced fertility and chronic pain. Impacting both the health and psycho-social functioning of millions of women worldwide, there is an urgent need for innovative non-hormonal, non-invasive treatments for the disorder. Both peritoneal and lesion-resident macrophages have been strongly implicated in the pathogenesis of endometriosis; key roles include promotion of lesion growth, neuroangiogenesis and nerve sensitization. With such a central role in the disease, macrophages represent a novel therapeutic target. In the current preclinical study, we sought to repurpose the macrophage targeting anti-cancer drug RRx-001 for the treatment of endometriosis. We utilised mouse models of induced endometriosis to demonstrate that RRx-001 acts to reduce endometriosis lesions and attenuate associated pain-like behaviours, without negatively impacting fertility. Using single nuclei multiome analyses, we identified a modification of macrophage subpopulations in the peritoneal cavity, specifically a reduced acquisition of a pro-disease phenotype and an accumulation of a pro-resolving phenotype. These observations signify the potential of RRx-001 as a novel therapeutic for endometriosis management.

52 **Introduction**

53 Endometriosis is a common, chronic, neuro-inflammatory condition that affects 1 in 10 women (and
54 those assigned female sex at birth) during their reproductive years, although adolescent and
55 postmenopausal cases are well documented(*1*). Endometriosis is defined by ectopic endometrial-like
56 tissue which forms non-neoplastic 'lesions', commonly within the peritoneal cavity and rarely (<1%),
57 in extra-pelvic locations(*2, 3*). Endometriosis has a complex and diverse symptomology which includes
58 severe dysmenorrhea, chronic pelvic pain, dyspareunia, fatigue, and infertility. These symptoms have
59 a cumulative impact on health, well-being, and psychosocial functioning. Beyond the personal impact
60 on those that suffer from the condition and that of their partners and family, endometriosis also
61 represents a substantial socioeconomic burden, due not only to the cost of treatment, but also as a
62 result of significant reductions in productivity(*4*).

63 Despite the high prevalence of endometriosis, there remains limited etiological understanding
64 of the disease(*5*). Sampsons' theory of retrograde menstruation is the most commonly accepted
65 hypothesis for the origin of endometrial-like tissue within the peritoneal cavity, referring to the reflux
66 of sloughed menstrual debris through the fallopian tubes during menstruation(*6*). Although
67 retrograde menstruation is common, occurring in 90% of those with patent fallopian tubes, only a
68 proportion develop endometriosis, indicative of a multifactorial pathogenesis, with immune
69 dysregulation prominent amongst many suspected etiological factors(*7-9*). Following an
70 immunological inability to eliminate refluxed ectopic endometrial fragments, adherence and cell
71 proliferation under hypoxic stress occurs, thus initiating the development of endometriotic lesions(*10,*
72 *11*). The current medical management of endometriosis is non-curative and includes analgesic
73 management, hormonal suppression, and surgical debulking of lesions(*12*). This current strategy is
74 insufficient due to common post-surgical recurrence of lesions, unwanted side-effects from hormonal
75 medications (anovulation and those associated with hypoestrogenism), and a high prevalence of
76 endometriosis-associated pain that is refractory to medical treatment(*13-15*). Thus, there is an urgent,
77 unmet need for novel non-hormonal therapeutics for endometriosis.

78 Macrophages have been strongly implicated in the promotion of endometriosis, emerging as
79 a potential target for a non-hormonal endometriosis therapy(*16*). These dynamic mononuclear
80 phagocytes are present in all tissues, playing integral roles in innate immunity, tissue homeostasis,
81 and the induction and resolution of sterile inflammation. Macrophages demonstrate considerable
82 transcriptional and phenotypical plasticity, existing on a broad spectrum between two highly polarised
83 states: pro-inflammatory and pro-repair, with a varied and dynamic functionality(*17*). Macrophage
84 function is dependent on both the perception of extracellular signals within the tissue niche and

85 cellular ontogeny: seeded pre-birth from the embryonic yolk sac/fetal liver, or monocyte-derived and
86 recruited from the circulation(*18, 19*).
87 In endometriosis, macrophages (and their precursors, monocytes) are an important
88 component of the intra- and extra-lesion microenvironment. They are continuously recruited and play
89 pathophysiological roles in lesion establishment, angiogenesis, and nociception(*20, 21*). In both
90 patients and animal models, pro-endometriosis macrophages have been demonstrated to trend
91 predominantly towards a pro-repair phenotype(*22, 23*). However, broad heterogeneity in peritoneal
92 and lesion-resident populations has been revealed in detailed analyses using techniques such as single
93 cell RNA-sequencing (scRNA-seq) and mass cytometry by time-of-flight (mass CyTOF), demonstrating
94 subpopulations across the spectrum, playing subtype-specific roles in the progression or regression of
95 endometriosis(*24-27*). An inability of macrophages to sufficiently recognise and clear refluxed ectopic
96 endometrial-like tissue, alongside deficient phagocytic capabilities, have been identified in several
97 endometriosis studies(*28*). In the peritoneal cavity of mice, the predominant macrophage populations
98 are small peritoneal macrophages (SpM) and large peritoneal macrophages (LpM), with monocyte-
99 derived LpM demonstrated to be protective against endometriosis development, possibly due to
100 enhanced lipid metabolism and cholesterol efflux, highlighting an intrinsic link between macrophage
101 ontogeny and functionality(*26, 29*). Conversely, endometrial-derived lesion-resident macrophages
102 enhance lesion growth(*26, 29*) and monocytes that are recruited directly to lesions from the
103 vasculature differentiate *in situ* into macrophages that exhibit a pro-disease phenotype(*26*).
104 Macrophages and monocyte subpopulations are also altered in the endometrium and peripheral
105 blood of women with endometriosis, suggesting systemic myeloid dysfunction(*30*).
106
107 Parallels in phenotype and function can be drawn between macrophages in endometriosis and solid
108 cancers. As with lesions, mononuclear cells are continuously recruited into tumour tissues where they
109 differentiate into macrophages. Niche specific factors, including hypoxic stress, lead to phenotype
110 specification and pro-disease functions and an attenuation of phagocytic capabilities(*31*). Tumour
111 associated macrophages (TAM) are broadly described as having a pro-repair phenotype, however,
112 similar to endometriosis macrophages, deep immunophenotyping has identified diverse TAM
113 subpopulations across the phenotypic continuum, including macrophages in highly phagocytic,
114 cytotoxic, and potentially anti-tumorigenic states(*32-34*). Paradoxically, when appropriately polarised,
115 tumour-resident macrophages can mediate cancer cell phagocytosis, and enhance tumour
116 clearance(*35*). Multiple anti-cancer immunotherapies that reprogram TAM have emerged in recent
117 years, aiming to alter pro-tumorigenic phenotypes and enhance tumour-clearing activity(*36*). Due to
118 the inherent similarities between the immunopathophysiology, and recent single cell analysis

revealing the presence of pro-disease TAM-like macrophages within endometriotic lesions(*26*), we have sought to repurpose the therapeutic strategy of macrophage repolarisation for endometriosis.

RRx-001 is a first-in-class small molecule inhibitor currently in several phase I-III clinical trials for a variety of solid cancers, with properties linked to multiple mechanisms of activity including macrophage modulation, phagocytic enhancement, vascular normalisation, inflammasome inhibition and epigenetic modifications, amongst others(*37*). In the current study, we have evaluated the impact of RRx-001 in preclinical mouse models of experimental endometriosis to determine the effect on endometriotic lesion growth and associated pain-like behaviours, and to identify any impacts on oestrous cyclicity and reproductive outcomes. As RRx-001 is known to modulate macrophage phenotype, we utilised 10x multiomic sequencing to investigate the transcriptomic and epigenetic landscape of peritoneal macrophages isolated from mice with induced endometriosis, dosed with or without RRx-001. Collectively, we describe vital preclinical data that indicates RRx-001 could be a promising new therapeutic for endometriosis

Results

RRx-001 reduced endometriotic lesion growth and attenuated pain-like behaviours in a 'menses' mouse model of experimental endometriosis. The impact of RRx-001 was evaluated in a syngeneic bioluminescent 'menses' mouse model of induced endometriosis. In brief, ovariectomised recipient mice received an intraperitoneal injection of 'menses'-like endometrium and oestradiol supplementation(*38*). Mice were randomly assigned to a treatment group and received either intravenous injection of RRx-001 or vehicle control, 6 hours prior to donor tissue transfer, and then twice weekly for 2 weeks (Fig.1A). *In vivo* bioluminescent imaging at days 3, 7, 10 and 14 was performed for continuous monitoring of lesions (Fig.1B). Spontaneous resolution and/or lesion progression was observed in the 'menses' model of endometriosis (as previously documented), leading to a high intragroup variability of bioluminescent signal(*38*). Despite the occurrence of some spontaneous resolution, there was no significant difference in bioluminescent signal across the vehicle group at different timepoints. Conversely, mice dosed with RRx-001 exhibited a reduction between days 3 and 7, and days 3 and 14 ($p=0.0079$ and $p=0.020$, respectively; Fig.1C). Lesions were recovered at day 14 and histologically verified (Fig.S1); mice dosed with RRx-001 exhibited decreased lesion number ($p=0.013$; Fig.1D) and a reduced cross-sectional lesion area (median = 1.48 mm^2), compared to vehicle control (median = 4 mm^2, $p=0.04$; Fig.1E). To determine if RRx-001 attenuated evoked pain-like behaviours, mechanical hyperalgesia was assessed using von Frey filaments on days 11, 12 and 13 post-lesion induction. Mice that received RRx-001 exhibited an increased abdominal retraction threshold ($p=0.0004$; Fig.1F), implying reduced abdominal sensitivity, possibly due to the resolution of

153 lesions within the peritoneal cavity. No differences were observed in hind paw withdrawal
154 measurements (Fig.1G).
155 We performed flow cytometry analysis on the peritoneal lavage of endometriosis mice
156 treated with or without RRx-001 and found no alteration in the abundance of LpM or SpM populations
157 (Fig.S2A and C-D). As RRx-001 has been reported to modulate macrophage phenotype, and was
158 previously found to attenuate expression of Sirpα(*39*) (receptor Sirpα-Cd47 ligand interaction
159 protects 'self' cells from phagocytosis), we investigated the expression of Sirpα on peritoneal
160 macrophages; expression was increased on LpM isolated from mice with induced endometriosis (p =
161 0.0046, Fig.S2B and E) and RRx-001 treatment attenuated Sirpα levels (p=0.0053, Fig.S2B and E).
162
163 **RRx-001 reduced endometriotic lesion growth and attenuated evoked *and* non-evoked pain-like**
164 **behaviours in a minimally invasive mouse model of experimental endometriosis.** To extend our pre-
165 clinical testing of RRx-001, we utilised an additional, complementary mouse model of endometriosis.
166 In this minimally invasive bioluminescent model, full thickness uterine fragments were injected
167 intraperitoneally into intact recipient mice. Lesions established in this model exhibit less spontaneous
168 regression and improved longevity(*38*), and since recipients are intact, post-incision pain sensitivity is
169 avoided allowing improved pain behaviour testing. Mice were randomly assigned to a treatment group
170 and received a full thickness tissue transfer (day 0). One week following lesion induction, mice were
171 dosed (day 8) with either RRx-001 or vehicle, and then twice weekly for 2 weeks (Fig.2A). Mice exposed
172 to RRx-001 exhibited a reduction in lesion bioluminescence from day 7 (pre-treatment) to day 21
173 (p=0.25; Fig2B, C). No reduction in bioluminescence was observed in the vehicle group. Lesions were
174 recovered at day 21 and histologically verified. The RRx-001 group had a reduced lesion number
175 (p=0.0056; Fig.2D) and a reduced cross-sectional area (median = 1.6 mm^2) compared to the vehicle
176 treated mice (median = 3.1 mm^2, p=0.020; Fig.2E).
177 To perform a comprehensive investigation into the impact of RRx-001 on endometriosis-
178 associated pain, we used multiple evoked and non-evoked behavioural tests at i) baseline (pre-
179 endometriosis induction), ii) after endometriosis induction but prior to treatment (days 7/8) and iii)
180 after RRx-001/vehicle treatment (days 17/18; Fig.2A). To determine if RRx-001 treatment led to an
181 attenuation of evoked pain-like behaviours, mechanical and thermal allodynia were assessed using
182 von Frey filaments and the hot plate test, respectively. We did not detect any significant differences
183 between groups prior to endometriosis induction (day -1/-2) or pre-treatment (day 7/8) across evoked
184 behavioural tests (Fig.3A-C). Post treatment, RRx-001 treatment led to a significant decrease in
185 mechanical allodynia, with increased withdrawal thresholds in both abdominal (p=0.002; Fig.3A) and
186 hind paw measurements (p=0.013; Fig.3B). A significant increase in hot plate latency at day 17 in RRx-

001 treated mice (p=0.0064; Fig.3C) was also detected. Next, we assessed the impact of RRx-001 on non-evoked pain-like behaviour using the ethologically relevant measures, thermal plate preference, burrowing and nesting. Burrowing and nesting are known to be reduced or eliminated with decreased well-being and can therefore be used as a surrogate marker of visceral pain evoked by endometriosis(*40*). Prior to endometriosis induction or pre-treatment at days 7/8, we did not detect any statistical differences between RRx-001 and vehicle groups in non-evoked behavioural tests (Fig.3D-F). Post treatment, thermal plate preference testing (TPPT) revealed a significant difference between groups at day 18 (p=0.005; Fig.3D) which may be indicative of a potential alleviation of hypothermal sensitivities following RRx-001 treatment. Of note, mice exhibited only exploratory behaviour on the cold plate, whereas the warm plate was also used for grooming by all mice, suggesting a thermal preference for warmth, as opposed to cold allodynia. No post-treatment differences were identified in burrowing behaviour between experimental groups (Fig.3E). RRx-001 treated mice did exhibit significantly increased nest complexity score (p< 0.0001, Fig.3F, representative nest images shown in Fig.3G) indicating improved well-being due to an attenuation of endometriosis-associated pain.

RRx-001 impacts the transcriptomic and epigenomic landscape of peritoneal macrophages in mice with induced endometriosis. 10x single nuclei multiomic profiling was used to generate paired RNA and ATAC libraries for sequencing to investigate the transcriptomic and epigenomic impacts of RRx-001 on peritoneal macrophages (Fig.4A). For this experiment, we used the 'menses' model of induced endometriosis, as the intraperitoneal injection of decidualised endometrial tissue most closely recapitulates the refluxed menstrual tissue thought to initiate endometriotic lesions. At day 7 post-lesion induction, fluorescent activated cell sorting (FACs) was utilised to isolate Lineage-, Cd45+ leukocytes from the peritoneal lavage of RRx-001 and vehicle treated endometriosis mice, as well as sham controls (n=9, n=5, n=3, respectively, Fig.S3A), followed by multiomic processing using the 10X pipeline. We performed an integrative analysis of peritoneal macrophages combining both modalities into a 'weighted-nearest-neighbour' (WNN) framework, with any cells identified as non-macrophages removed (Fig.S3B-E)(*41*). UMAP projection revealed 7 macrophage clusters; inset shows the samples split by library ID (Fig.4B). We found consistent weighting of RNA and ATAC across clusters (although an increased RNA modality weight was seen in the proliferative cluster), uniformity of high-quality nucleosome signal (ATAC) and a consistently high log10GenesPerUMI (RNA) (Fig.S3C). All peritoneal macrophage clusters were *Cd45*+ and *Cd11b*+, and our feature plots of *H2-Ab1* and *Adgre1* enable visualisation of SpM by low *Adgre1* (F4/80) and high *H2-Ab1* (MHCII) expression, prototypical LpM

220 with high *Adgre1* and low *H2-Ab1*, and intermediate *Adgre1* in other LpM populations, as previously
221 characterised in mice with induced endometriosis at the single cell level(*26, 42*) (Fig.4C).
222 An analysis of sample composition by cluster revealed macrophage subpopulations were
223 shared between experimental groups. Prototypical LpM (defined by *Timd4* and characteristic DEGs
224 *Prg4*, *Ltbp1*, *Alox15*) exhibited comparable proportions in each sample, as did proliferative LpM and
225 SpM. The predominant population in the vehicle treated endometriosis mice, termed pro-disease
226 LpM, expressed the DEGs *F13a1, Gas6, Lyve1* and *Nrp1*, previously linked to endometriosis(*30, 42*),
227 this population was markedly reduced in both RRx-001 treated and sham mice (Fig.4D,E). In RRx-001
228 treated mice, the predominant population was termed pro-resolving LpM due to the associated lesion
229 resolution observed and the expression of genes such as *Ms4a4*, *Ccr2*, *Calhm6*, *Fcrla* and *Saa3*
230 associated with inflammatory monocyte-derived infiltration, response to pathogens / antigens and
231 lipid-associated phenotypes, previously linked to lesion resolution (Fig.4D,E)(*26, 29*). We included
232 sham mice in this analysis, which exhibit a post-surgical loss and subsequent replenishment of
233 prototypical LpM and therefore model a resolution of transient inflammation. As expected, transitory
234 LpM were predominant in sham mice; both populations expressed intermediate levels of *Adgre1* and
235 *Timd4* and were separated by enhanced *Vsig4* expression (in transitory LpM 1; Fig.4D,E), a gene known
236 to represent longer time-in-residency, suggesting transitory LpM1 have been present in the peritoneal
237 niche longer than transitory LpM2(*43*).
238 Abundant expression of *Ccr2* and low *Timd4* on SpM and pro-resolving LpM indicated recent
239 recruitment/monocytic-derivation of these populations, an ontogeny previously shown to be
240 protective against endometriosis development(*29*); paired ATAC data also demonstrated increased
241 chromatin accessibility of the *Ccr2* gene in these populations and significant peak-gene links (Fig.4F).
242 Top DEGs separating pro-resolving and pro-disease LpM were those linked with monocytic ontogeny
243 and complement protein C1q as well as *Saa3* (Fig.4G). Enhanced mRNA levels of the transcription
244 factor, *Cebpb* (associated with regulating macrophage lipid metabolism and phagocytosis(*44*)) were
245 evident in the pro-resolving population (Fig.4G), suggesting enhanced Cebpb regulation of this
246 phenotype. Conversely, transcription factor footprinting did not support this; with comparable
247 enrichment observed in pro-resolving, pro-disease and prototypical populations. Expected
248 footprinting differences, such as the characteristic Gata6 control of prototypical LpM, were detectable
249 in the ATAC data, with most enrichment observed in prototypical LpM and least enrichment observed
250 in pro-disease LpM (Fig.4H)(*45*). We also performed DNA sequence motif enrichment analysis of the
251 ATAC data to identify overrepresented motifs in the differentially accessible peaks of RRx-001 treated
252 mice (all macrophages), with hypergeometric probability testing of enrichment against a set of
253 background peaks matched for GC content. We identified a strong enrichment of Kruppel-like factor

motifs (Klf15, Klf14, Klf2), with Klf family members having broadly reported roles in the activation and polarisation of macrophages, recent research has identified highly specific and unexpected roles in macrophage differentiation for these broadly expressed transcription factors(*46*). The greatest overrepresentation was seen in the Klf14 (4.03-fold enriched, $p < 0.0001$) and Klf15 (2.91-fold enriched, $p < 0.0001$) motifs, which alongside Klf2, have been linked to modulation of inflammatory signalling pathways. Sp4 and 9 motifs were also enriched (3.06-fold and 2.96-fold enrichment respectively). Of particular interest was the enrichment of Nrf1 motifs (5.29-fold enrichment, $p<0.0001$); RRx-001 has previous been shown to induce Nrf2 which mediates an antioxidant response(*47*). Nrf1 works in concert with other transcription factors such as Nrf2 to modulate cellular responses to oxidative stress and maintain cellular homeostasis.

Next, slingshot was used to perform cell lineage and pseudotime inference analysis on reduced dimensional data using previously identified WNN clusters. SpM was specified as the initial cluster as the infiltration and transformation of monocytes into SpM with eventual differentiation into LpM is known to occur under inflammatory conditions, such as endometriosis. Lineage inference identified three branching trajectories from SpM (Fig.5A)(*23*); pseudo-temporal trajectories to the terminal populations of pro-disease LpM, prototypical LpM and proliferative LpM were identified. Interestingly, pro-resolving LpM appeared to be an intermediate in all trajectories, further supportive of a recent monocyte-derived ontogeny for this population (Fig.5B). Multinomial logistic regression was used to assess the pseudo-temporal sample imbalance in individual lineages, while adjusting for baseline sample probabilities. Macrophages from sham mice were more likely to be enriched further along in the pseudotime trajectories of both prototypical and proliferative lineages, as expected due to a greater replenishment post transient inflammation and were less likely to be present in the pro-disease LpM lineage. Macrophages from vehicle treated mice were most abundant in the pro-disease lineage and predominant across all pseudotime points indicating increased pro-disease differentiation (Fig.5B). Conversely, in RRx-001 treated mice, macrophages were present at earlier pseudotime points in the prototypical and proliferative lineages and were also less present in the pro-disease LpM lineage, suggesting a reduction in pro-disease phenotypical differentiation. These data led us to conclude that RRx-001 appears to prevent the acquisition of pro-disease phenotype. As our analysis revealed pseudo temporal differences at early pseudotime points, we performed an aggregate analysis of the LpM and SpM populations from RRx-001 and vehicle mice which also indicated differences in SpM gene expression (Fig.5C). To further probe these differences, we performed gene set enrichment analysis with ClusterProfiler using GO terms (RRx-001 vs Vehicle), and identified terms related to activation of macrophages, antigen processing and defence responses (Fig.5D). Furthermore, KEGG pathways suggested an enhancement of phagosome and lysosomal activity,

288 alongside antigen processing, with the majority activated in both the LpM and SpM populations (Fig.
289 5E), supporting the concept that treatment of induced endometriosis with RRx-001 may impact
290 peritoneal myeloid populations early in the differentiation trajectory. In line with RRx-001 enhancing
291 phagocytic activity in macrophage populations we demonstrated reduced average expression level of
292 Sirpα in transcriptomic and gene activity data (inferred from ATAC) compared to vehicle treated mice,
293 corresponding with our flow cytometric analysis at day 14 (Figs.5F, S1C) and indicating that RRx-001
294 acts to disrupt the Sirpα-CD47 immune evasion signal that is enhanced in endometriosis.
295
296 **RRx-001 does not impact reproductive function in mice.** The therapeutic activity of RRx-001 has been
297 safely evaluated in over 300 patients with no increase in infections or anaemia detected, indicating
298 limited side-effects. Impact on reproductive function has not yet been evaluated(*37*). Currently, gold-
299 standard treatment of endometriosis focuses on surgical intervention or therapeutic ovarian
300 suppression (oral contraceptives/GnRH agonists). A non-hormonal medical alternative that does not
301 interrupt reproductive function is urgently needed. To this end, we sought to determine if pre-
302 pregnancy treatment with RRx-001 led to any aberrant changes to fertility or developmental impacts
303 in mice. Pre-pregnancy intravenous dosing was chosen for these initial experiments as an RRx-001-
304 bound haemoglobin adduct persists for the lifetime of the red blood cell, reported to be 40.7 ± 1.9
305 (S.D) days in mice, potentially leading to long-term impacts(*48*). Tissue-resident endometrial
306 macrophages dynamically regulate tissue homeostasis and remodelling during the oestrous cycle in
307 mice(*49*), thus we initially investigated the impact of RRx-001 on oestrous cycle length, and within
308 individual stages, to identify any perturbations. Oestrous cycles were synchronised using the Whitten
309 effect(*50*), followed by daily staging by wet vaginal cytology preparations for > 4 complete cycles prior
310 to treatment with either RRx-001 or vehicle for 1-week. Daily staging continued for > 4 further cycles.
311 No significant changes in overall cycle length or individual cycle stage were detected in RRx-001
312 treated mice pre- or post-treatment (Fig.6A, B).
313 Next, mice were dosed with RRx-001 or vehicle for 1-week, with harem breeding set up 24-
314 hours post final drug dose for investigations into reproductive function. Within these experiments,
315 pregnancy success rates following copulatory plug detection were as expected within breeding
316 colonies: 13/16 RRx-001 treated mice became pregnant (1 did not plug, 2 not pregnant post-plug) and
317 14/15 vehicle treated mice became pregnant (1 not pregnant post-plug). Sexual receptivity was
318 assessed by daily seminal plug checks, detected between 0.5 - 4.5 days post-mating. No significant
319 differences in time to seminal plug were observed (Fig.6C). At embryonic day (E)10.5, no significant
320 differences in average embryo number or embryo weight were determined between experimental
321 groups (Fig.6D, E). At E15.5, Hofbauer cells, a heterogenous population of placental macrophages

322 which broadly exhibit a pro-repair phenotype, were isolated from the chorionic villus of the foetal
323 placenta and assessed using quantitative spectral flow cytometry. We sought to assess Hofbauer
324 phenotype; dysregulation of these cells is associated with placental pathologies including inadequate
325 development, inflammation and infection(*51*). No significant differences were identified in the MFIs
326 of SIRPα, CD206 and CD40 between RRx-001 and vehicle groups (Fig.6F). As expected for a
327 predominantly pro-repair population, CD206 was expressed across both experimental groups, with no
328 expression of pro-inflammatory CD40.

329 Finally, the remaining pregnant mice and pups were monitored throughout pregnancy and
330 during the postnatal period. We found no impact of RRx-001 on gestational length (Fig.6G).
331 Furthermore, mice treated with RRx-001 did not have any alterations to number of pups (ranging from
332 2-11 in the vehicle group, and 3-11 in the RRx-001 treated group; Fig.6H), or sex ratio of litter (Fig.6I).
333 Post parturition, mothers remained healthy and omental milk spots were observed in all pups on day
334 1 indicative of successful lactation and nursing. Pups were weighed at postnatal day 7, with weekly
335 weighing up to 28 days of age, with no significant differences detected at any timepoint (Fig.6J).
336 Collectively, these data indicate that RRx-001 does not impact reproductive function.

337

338 **Discussion**

339 In the current study we have revealed that RRx-001 has a robust therapeutic impact in mouse models
340 of induced endometriosis; treatment decreased lesion number and size, and attenuated pain
341 associated behaviours. Using multiomic single nuclei sequencing we determined an evident impact on
342 macrophage populations whereby the abundance of pro-disease macrophages was reduced, and the
343 proportion of pro-resolving macrophages was enhanced. Trajectory analysis inferred that RRx-001
344 tips the balance in favour of pro-resolving macrophage by preventing differentiation to a pro-disease
345 phenotype. Finally, preliminary investigations into reproductive function suggest that RRx-001 does
346 not impede fertility or aberrantly affect embryonic development *in utero.* Taken together, we present
347 promising preclinical data highlighting RRx-001 as novel macrophage directed therapy for the
348 treatment of endometriosis.

349 In the 'menses' model of induced endometriosis we found that when treatment with RRx-001
350 was initiated prior to establishment of lesions, there was no difference in bioluminescent signal
351 between vehicle control and drug treated mice on day 3, indicating that RRx-001 does not impact the
352 initial stages of ectopic endometrial tissue adhesion within the peritoneal cavity. This aligns with the
353 proposed erythrophagoimmunotherapeutic activity of RRx-001; in which the covalent encapsulation
354 of RRx-001 in red blood cells vectors RRx-001 to hypoxic (tumour) vasculature – leading to vasculature
355 occlusion, haemolysis and erythrophagocytosis by tumour associated macrophages(*39*). This

356 phenomenon may also be occurring in lesions, which are also exhibit hypoxic areas, following the
357 initial stages of vascularisation that occur in the first week(*52*). Interestingly, in the menses model,
358 RRx-001 treatment led to a reduction in bioluminescent signal between days 3 to 7 and days 3 to 14,
359 but not day 3 to 10, this may be related to cases seen in the treatment of lung cancer with RRx-001,
360 when tumour pseudo-progression is detected early in treatment due to tumoral lymphocyte
361 infiltration, before regression occurs later, leading us to hypothesise that this may also be occurring
362 within the endometriotic lesions(*52*). Future studies will establish the dynamics of pseudo-progression
363 if present, and determine the regime required for elimination of lesions.

364 We also investigated the impact of RRx-001 in a minimally invasive model of induced
365 endometriosis; we previously determined that endometriotic lesions established using this model
366 exhibit greater longevity(*38*). In this model, full thickness uterine fragments are transferred containing
367 myometrial tissue, and resulting lesions are usually larger than in the menses model and have a cystic
368 appearance. We used two alternate models in this study to model alternate 'phenotypes' of
369 endometriosis, with the minimally invasive model representing a more persistent form of
370 endometriosis. Here, we also demonstrated a significant reduction in lesion growth when treatment
371 was initiated 1-week post-lesion induction, rather that prior to lesion induction, again indicative that
372 RRx-001 resolves established lesions. In both models, treatment with RRx-001 led to an attenuation
373 of abdominal mechanical hyperalgesia, indicative of reduced pain in this region and perhaps due to
374 the accompanying resolution of lesions with treatment. We also included non-evoked behavioural
375 tests as they better recapitulate impacts to well-being that are associated with endometriosis and are
376 used as surrogate measures of visceral pain. The inclusion of non-evoked behavioural tests were
377 described recently as an absolute requirement in the replication and translation of the complex pain
378 experience of endometriosis patients(*40*). In our studies, nest building(*53*) was the most sensitive
379 assay for identifying behavioural phenotypes; impaired nest building was seen in mice at day 7 post-
380 lesion induction. Following treatment with RRx-001 nest building was restored to a quality beyond
381 that observed in naïve, pre-endometriosis mice.

382 Our multiomic analysis revealed that RRx-001 leads to a reduction in pro-disease LpM and an
383 accumulation of pro-resolving LpM (prototypical LpM remained constant in each group (sham, RRx-
384 001, vehicle). Since our trajectory analysis suggested that the pro-resolving LpM phenotype is a
385 transitory cell state we predict that RRx-001 prevents the acquisition of a pro-disease phenotype by
386 newly recruited monocyte-derived LpM. The transcriptional phenotype of pro-resolving LpM
387 exhibited some similarities to that of monocyte-derived LpM observed in our previous studies(*26*)
388 which were attributed to protective functions in the mouse model of endometriosis. DEGs include
389 lipid associated genes and those encoding C1q; suggesting roles in the reduction of available lipid,

390 hormone synthesis and activation of membrane lytic complexes. Treatment with RRx-001 also
391 appeared to increase genes associated with response to pathogens and antigens suggesting improved
392 visibility of ectopic tissue to peritoneal macrophages.
393
394 Together these may reduce endometriosis drivers and promote destruction of ectopic tissue. RRx-001
395 has previously been shown to have significant impacts on the epigenome of cancer cells; effects vary
396 depending on the dose and timepoints evaluated - sites that were hypo- and hyper-methylated as well
397 as globally increased acetylation were reported(*54*). We predict that in the peritoneal cavity RRx-001
398 prevents acquisition of pro-disease phenotype via epigenetic modification. Of particular interest, we
399 found that Klf (including Klf14) binding motifs were enriched in peritoneal macrophages derived from
400 mice exposed to RRx-00. Previous studies have identified a role for Klf14 in reducing glucose
401 metabolism and immune function in macrophages; this seems to exert a protective function in
402 inflammatory conditions by limiting inflammatory cytokine secretion(*46*). These modifications also
403 highlight the paradoxical nature of RRx-001 mechanisms reported in the literature, whereby
404 antigenicity is enhanced whilst simultaneously promoting an antioxidative and anti-inflammatory
405 environment.
406 Much of the research conducted on the mechanism of action of RRx-001 has occurred in the
407 oncology field, where studies describe targeting of RRx-001 to hypoxic and aberrant vasculature
408 prevalent within tumours via binding to haemoglobin within red blood cells. Drug bound RBCs travel
409 to hypoxic vasculature where they accumulate because of their RRx-001 induced rigidity(*55*). During
410 this process, nitric oxide (NO) is released which is thought to confer cytotoxic activity within
411 tumours(*56*). Macrophages also engulf RRx-001 bound RBCs, inducing polarisation from a pro-repair
412 to pro-inflammatory state and down-regulating the CD47-SIRPα pathway, which reduces tumour cell
413 immune evasion(*57, 58*). Immunogenicity of cancer cells is also induced via increased expression of
414 interferon (IFN)-responsive genes(*59*). Given the similarity that exist between cancer and
415 endometriosis (including pro-disease macrophage polarisation and pathological immunotolerance)
416 and that endometriosis lesions also exhibit a hypoxic environment, we predict that significant RRx-001
417 impacts are also occurring within lesions. Future work will interrogate the intra-lesional environment
418 in response to RRx-001. The mediation of indirect effects within associated environments has not yet
419 been characterized, however from our results it is plausible to suggest that the modulation of
420 macrophage populations within the peritoneal cavity occurs as a secondary outcome resulting from
421 endometriotic lesion resolution by lesion-resident macrophages subsequently reducing the
422 inflammatory burden within the peritoneal cavity, modified cytokine signalling from intra-lesional
423 immune cells, the release of reactive oxygen and nitrogen species, or a combination of these impacts.

424 Thus, further work is required to elucidate the impacts of RRx-001 on lesion-resident macrophage
425 populations, including interrogation of off-target effects in other tissues.
426 Our initial results evaluating fertility in mice exposed to RRx-001, indicate that pre-pregnancy
427 treatment with RRx-001 does not impair the normal reproductive function of female mice or embryo
428 development indicating that it has potential suitability as a non-hormonal and fertility sparing
429 treatment for endometriosis. Further work will identify whether RRx-001 can rescue endometriosis-
430 associated infertility.
431 To summarize, we have revealed a novel indication for the anti-cancer drug RRx-001 in the
432 treatment of endometriosis. It acts to reduce endometriosis lesions, associated pain-like behaviours
433 and modulates macrophage populations in the peritoneal cavity without negatively impacting fertility.
434 RRx-001 is currently in phase I - III clinical trials for different solid cancers, is well tolerated with
435 available safety data. In this first phase of preclinical testing, we highlight a robust effect in
436 experimental endometriosis and plan to proceed to a feasibility trial in women with the disorder. RRx-
437 001 and its macrophage modifying actions has the potential to improve the lives of millions of women
438 suffering from endometriosis.
439
440 **Acknowledgements**. The authors thank Dr Laura Baxter at the Bioinformatics RTP, University of
441 Warwick, for pre-processing of multiomic data. We would also like to thank Deborah McIntyre for the
442 independent quantitative scoring of nests. The authors acknowledge the use of flow cytometers and
443 technical expertise provided Dr Steven Servin and Dr Sarah Bennett, in the flow shared laboratories
444 resource (FlowSRL), University of Warwick.
445
446 **Funding**. This work was supported by an MRC iCASE (Ferring Pharmaceuticals were the industrial
447 partner and provided additional funding for consumables and travel) studentship to I.M and an MRC
448 Project Grant (MR/S002456) to E.G. The authors declare no conflict of interest.
449
450 **Author contributions:** E.G conceptualised and supervised the study and acquired funding. I.M
451 conducted animal experiments, analysed data, and performed multiomic analyses. V.V performed
452 multiomic analyses. C.L.P and M.R performed experiments and analysed data. P.D and K.P performed
453 animal experiments. I.M and E.G wrote the manuscript.
454
455 **Data and materials availability:** All data associated with this study is present within the manuscript
456 and the included supplementary materials. Analysis script for both multiomic and cross-species

457 analyses are publicly available on github.com under project x. Multiomic sequencing data are
458 deposited in Gene Expression Omnibus under accession number x.
459
460 **Materials and Methods**
461 **Study design**. These experiments were designed to determine the impact of RRx-001 treatment in a
462 mouse model of experimental endometriosis and to identify any potential impact on fertility
463 outcomes. For the purpose of determining the impact of RRx-001 on induced endometriosis, we
464 implemented two complementary mouse models ('menses'(*60*) and 'minimally-invasive'(*38*)) in which
465 to robustly examine endometriotic lesion growth and pain-like behaviours. Additionally, we utilised
466 multiomic sequencing to determine transcriptomic and epigenomic effects of RRx-001 on peritoneal
467 macrophages isolated from the 'menses' mouse model. To assess fertility outcomes, we examined the
468 effect of pre-pregnancy dosing of RRx-001 on the oestrous cycle and reproductive functions. Animals
469 were randomised to either RRx-001 treatment or control group using the GraphPad QuickCalcs online
470 tool (https://www.graphpad.com/quickcalcs/randomize1/). Behavioural experiments were
471 performed under blinded conditions. Details of mouse models, sample size and statistical methods
472 are described in the appropriate sections below.
473
474 **Animals**. Wild-type FVB/N mice were purchased from either Envigo (Cambridge, UK) or Charles River
475 (UK) and maintained under standard conditions at the University of Warwick, UK. FVB-Tg(CAG-luc,-
476 GFP)L2G85Chco/J (stock number 008450|L2G85) were originally purchased from The Jackson
477 Laboratory (Bar Harbor, ME, USA), and a breeding colony maintained under standard conditions at
478 the University of Warwick. Mice were housed in standard conditions with a 12:12 light-dark cycle, an
479 ambient temperature of 21°C, humidity at 50%, and *ad libitum* access to food (standard rodent chow)
480 and water. The diet of weanlings was supplemented by apple sauce. Following arrival to the facility,
481 mice acclimatised for one week prior to commencement of experimental procedures. All procedures
482 performed were permitted under license by the United Kingdom Home Office Animal Experimentation
483 (Scientific Procedures) Act; PPL PP0568394, and in accordance with the guidelines of the Committee
484 for Research and Ethical Issues of the International Association for the Study of Pain.
485
486 **Mouse models of experimental endometriosis.** We implemented two variations of the
487 bioluminescent syngeneic mouse models of induced endometriosis; a 'menses' model and a minimally
488 invasive model, described in detail previously(*38, 60*). In brief, for the 'menses' model, recipient FVB/N
489 mice (n=24) were ovariectomised and received an intraperitoneal injection of decidualised and
490 progesterone withdrawn donor endometrium recovered from FVB/Cag-Luc mice (~40mg, minced,

491 resuspended in saline and passed through an 18 g needle) and exogenous oestradiol supplementation
492 (oestradiol valerate 500 ng, twice weekly). Surgical controls, referred to as 'sham' mice, were
493 ovariectomised FVB/N mice that received intraperitoneal injection of saline instead of tissue. In the
494 minimally invasive model, intact recipient FVB/N mice (n = 32) received an intraperitoneal injection of
495 FVB/Cag-Luc donor full-thickness uterus (equivalent to 1 uterine horn per recipient, minced and
496 passed through an 18 g needle). Oestrus stage was determined in donors and recipients by vaginal
497 smear and retrospective cytological analysis(*61*)
498 **Experimental groups**. Mice with induced endometriosis were randomly assigned to either (1) RRx-001
499 treatment or (2) vehicle control group. In the bioluminescent experiments, groups included were (1)
500 induced endometriosis and RRx-001 treatment ('menses' model n=13, minimally invasive model
501 n=16), or (2) induced endometriosis and vehicle control ('menses' model n=11, minimally invasive
502 model n=16), with dosing schedules as indicated in experimental schematics. In the 10x multiome
503 experiment, groups included were (1) induced endometriosis ('menses') and RRx-001 treatment (n=9),
504 (2) induced endometriosis and vehicle control (n=5), and (3) sham (n=3). In the fertility experiments,
505 mice were randomly assigned to either the (1) RRx-001 treatment (n=20), or (2) vehicle control group
506 (n=18), with sample size and dosing schedules as described within the results for individual
507 experiments. In all our studies, RRx-001 (Selleck Chemicals, USA) was dosed intravenously at 10mg/kg
508 in DMA:PEG-400 1:2, diluted 1:4 in sterile saline immediately prior to injection, 2x weekly (Monday
509 and Thursday, 12pm), with control mice receiving intravenous vehicle only.
510
511 **Non-invasive *in vivo* bioluminescence quantification**. As described previously, mice were injected
512 subcutaneously with 1.5 mg D-Luciferin Potassium Salt (75mg/kg, reconstituted in sterile PBS and
513 sterilised by 0.22 µm filtration), following a 5-minute period to allow a maximal luciferase signal
514 plateau, mice were imaged under maintained anaesthesia using a PhotonIMAGER (Biospace Lab,
515 Paris)(*38*). Lesion bioluminescence was measured using a standard region of interest across
516 experiments, on the front and back of each mouse for 7 minutes per side. Using M3 Vision software
517 (Biospace Lab), the background reading was subtracted, front and back readings averaged, and
518 photons/s/cm2/sr calculated for bioluminescent signal quantification.
519
520 **Histological and ImageJ analyses**. Post tissue fixation and embedding in paraffin, 3 µM sections of
521 recovered lesions were stained using a standard haematoxylin/eosin protocol. Images were taken on
522 a LeicaDMI microscope (Leica, Germany), with white balance and histological verification of
523 endometriotic lesion hallmarks (stroma +/- glandular epithelium) conducted in FIJI (ImageJ2, Version
524 2.3.0). In FIJI, analysis to determine cross-sectional area was performed on lesion images captured

525 using 4x magnification, image scale was set to a known size and the 'select' tool was implemented to
526 outline the lesion while excluding peritoneal wall/adipose tissue, and the 'measure' function was then
527 used to calculate cross-sectional lesion area.
528
529 **Behavioural assessments**.
530 *von Frey*. We determined mechanical allodynia as an average of measurements taken on days
531 11/12/13 post lesion induction ('menses' model) or day -1 (baseline), 8 (1 week; initiation of
532 treatment) and 18 (10 days following start of treatment; minimally invasive model) using calibrated
533 Semmes-Weinstein von Frey filaments (Stoelting, Wood Vale, IL, USA), as described previously(*38, 62*).
534 Briefly, mice were allowed to adapt to the apparatus until exploratory responses ceased. Filaments
535 were then applied 10 times in ascending order to the abdomen or hind paw. The filament force
536 (grams) was recorded when withdrawal responses were observed in 50% of applications
537 *Hot plate.* Thermal hyperalgesia was determined prior to lesion induction, and on day 7 and day 17
538 post-lesion induction using a hot plate (Ugo Basile, Italy). Mice were positioned onto a preheated plate
539 set at 52°C and their responses were observed. A time-to response (seconds) was noted when mice
540 exhibited a reaction to the thermal stimulus. If no response was observed within 25 seconds, the mice
541 were removed from the plate.
542 *Thermal plate preference.* Thermal hyperalgesia was determined prior to lesion induction, and on day
543 7 and day 17 post-lesion induction using TPP thermal place preference plates (Ugo Basile, Italy). The
544 thermal plates were set at distinct temperatures, one at 12.5°C and the other at 30°C. Mice were
545 allowed a 15-minute-period for exploration of both plates, during which the duration spent at 12.5°C
546 was recorded.
547 *Burrowing.* The ethological rodent behaviour of burrowing was determined prior to lesion induction
548 and on day 8 and day 18 post-lesion induction. Mice were individually supplied with a burrowing tube
549 (diameter 6.8 cm, length 20 cm), made of clear acrylic, open and elevated by 3 cm at one end to
550 prevent the accidental displacement of burrowing substrate (tubes manufactured at Life Sciences,
551 University of Warwick). The mouse was placed in a plastic cage with the burrowing tube filled with
552 110g of wooden shredding; following a one-hour burrowing assay, the material remaining was
553 weighed and recorded, and the percentage of material displaced within an hour calculated.
554 *Nesting.* The ethological rodent behaviour of nesting was determined prior to lesion induction and on
555 day 8 and day 18 post-lesion induction as described(*53*). Briefly, 1 hour prior to dark phase, mice were
556 individually housed with wooden shredding and a Nestlet (VetTech, UK). The following morning, the
557 nest is imaged, and the quality of the nest created from the shredded nestlet is recorded with a rating
558 scale of 1-5. (e.g. 1 no nest; 5 fully shredded material arranged into a neat nest). Mice had *ad libitum*

559 access to food and water during the test and were re-grouped immediately following the nesting assay
560 (Table S1).
561
562 **Flow cytometry**. Peritoneal lavage was collected into 5 ml of ice-cold DMEM, red blood cells were
563 lysed (name) and cells filtered through a 40 µM filter and then blocked with monocyte block (name)
564 prior to resuspension and staining of 1 million cells per sample with the antibody panel shown.
565 Samples were analysed using a FACS Aria Fusion with FACS Chorus software (BD Biosciences) and
566 FlowJo v.9 software. Hofbauer cells were isolated from the foetal placenta of mouse embryos at E15.5.
567 Dissection of the foetal placenta from embryonic yolk sacs and subsequent placental digestion into a
568 single cell suspension were performed as described previously, with three foetal placentas pooled
569 from each mouse(*63, 64*). Samples were filtered, RBCs lysed, blocked, and resuspended as above, prior
570 to staining of 1 million cells per sample with the antibody panel. Samples were analysed on a Sony
571 spectral ID7000 spectral cytometer (Sony Biotechnology, USA).
572

Marker	Fluorophore	Clone	Supplier	Product Number
CD45	Pacific Blue	30-F11	Biolegend	103125
Sirpα	BV510	P84	Biolegend	144005
Ly6C	BV711	HK1.4	Biolegend	128037
CD40	FITC	3/23	Biolegend	124607
c-kit	PerCP Cy5.5	ACK2	Biolegend	135133
CD163	PE	S15049F	Biolegend	156703
CD34	PE-Cy5	MEC14.7	Biolegend	119311
CD206	PE-Cy7	C068C2	Biolegend	141719
Lineage exclusion	APC		Biolegend	
CD19		1D3/CD19		152410
CD3		17A2		100235
CD335		29A1.4		137607
Ly6G		1A8		127613
SiglecF		S17007L		155507
MHCII	APC-Cy7	M5/114.15.2	Biolegend	107627
F4/80	APC Fire750	BM8	Biolegend	123117
Live/Dead	Zombie UV	-	Biolegend	423107

573

574 **Preparation of peritoneal immune cells for 10X multiomic sequencing**. Peritoneal lavage was pooled
575 within experimental groups (endometriosis/RRx-001 n=9, endometriosis/vehicle n=5, and sham n=3)
576 prior to processing and staining as described above, with fluorescence activated cell sorting based on
577 surface marker expression (Lin-/Cd45+) performed to enrich samples for macrophage populations.
578 100,000 cells per sample were sorted into 1ml PBS + 2% FBS using a FACs Aria. Gentle nuclei isolation
579 was performed, and nuclei were then processed and barcoded according to the established pipelines
580 to generate individual paired RNA and ATAC libraries using a 10x Nuclei Isolation Kit, a 10x Multiome
581 Kit and 10x Chromium Controller™ (10x Genomics). Libraries were sequenced individually by the
582 Genomics Lab at the University of Warwick on high-output 150 cycle cartridges using a NextSeq
583 500/550 (Illumina®, San Diego, USA).
584
585 **Bioinformatic analysis**. We followed recent guideline best practices for single cell analysis across
586 modalities as described by Heumos et al for our paired analysis of snRNA-seq and snATAC-seq
587 libraries(*65*). BCL files for each flow cell directory from the ATAC and GEX sequencing runs were
588 demultiplexed using Cell Ranger ARC analysis pipelines to generate FASTQ files. Seurat (5.0.3) and
589 Signac (1.13.0) in R studio (4.3.2) were used to create Seurat objects (v3) based on GEX data, with
590 ATAC-seq data added as a second assay. Using ATAC-seq data, a common peak set was created and
591 peaks were called in individual samples using MACS2 v2, with peaks on non-standard chromosomes
592 and in genomic blacklist regions removed(*66*). Independent quality filtering of each dataset was
593 performed on both modalities to remove low-quality cells based on number of detected molecules for
594 each modality, the number of genes detected per UMI, nucleosome signal and TSS enrichment. As
595 described in datasets generated by Yoshimura et al and 10x Genomics, the gentle nuclei isolation
596 protocol allows mitochondria to attach to the nuclei prior to GEM generation resulting in a high
597 mitochondrial percentage(*67*). Post-matrix generation we filtered reads aligned to mitochondrial or
598 ribosomal regions, and matrices were then subset on common genes. Finally, the scDblFinder and
599 SoupX were used to identify and remove doublets and assess ambient contamination, respectively(*68,*
600 *69*). Pre-processing of RNA datasets was performed using the SCTransform v1 workflow (Seurat),
601 followed by conservative anchor-based RPCA-integration using the default k.anchor parameter (5) to
602 align populations (Seurat). We then computed the LSI of individual peak datasets using standard
603 functionalities (Signac), followed by Harmony integration of datasets(*70*). The Seurat v4 weighted
604 nearest neighbour (WNN) method of 'FindMultiModalNeighbors' was utilised to compute a joint
605 neighbour graph to represent both the GEX and ATAC modalities, followed by the use of standard
606 workflows for WNN UMAP visualisation and clustering (Seurat). Clusters were identified using marker
607 genes identified in Wilcoxon rank-sum tests in a one-vs-all fashion for manual annotation according

608 to our previously published annotations of mouse peritoneal macrophages(*26*). Clusters
609 corresponding to non-macrophage populations or expressing < 1% of total cells were removed in order
610 to isolate 11,877 peritoneal macrophages (Fig.S3B, C). To account for within-sample correlation we
611 implemented MAST, a generalised mixed effect model, for differential gene expression testing(*71*).
612 Differentially accessible peaks were identified utilising logistic regression within the Signac
613 'FindMarkers' function. DNA sequence motif information (JASPAR2020) was added using the
614 'AddMotifs' function, with enriched motifs identified using 'FindMotifs'.
615 For data visualisation purposes the Seurat and Signac functionalities 'DimPlot', 'FeaturePlot',
616 'DotPlot', 'CoveragePlot', 'CellScatter', 'VlnPlot', 'MotifPlot', and the EnhancedVolcano package were
617 implemented(*72*) (*73, 74*). The clusterProfiler package was used for statistical analysis, output
618 simplification and visualisation of GO and KEGG terms(*75*). For trajectory analysis, DynGuidelines was
619 utilised to select the most applicable package and the indicated Slingshot package were
620 implemented(*76, 77*).
621
622 **Statistics**
623 Statistical analyses were performed using GraphPad Prism 10.1.1 for macOS (San Diego, CA). All
624 graphical data plotted as mean with standard deviation. For data meeting the necessary assumptions
625 for parametric analyses (Shapiro-Wilk), Student's t-tests or two-way analysis of variance (ANOVA) with
626 post hoc testing conducted with the Bonferroni test. If non-normality of data was detected, non-
627 parametric analyses were performed using a Mann-Whitney *U* test. Statistical significance for all tests
628 was established at $P < 0.05$. Significance levels were denoted as follows: * $P < 0.05$, ** $P < 0.01$, *** P
629 < 0.001, **** $P < 0.0001$.
630
631
632
633
634
635
636
637
638
639
640
641

642 **Figures and legends**

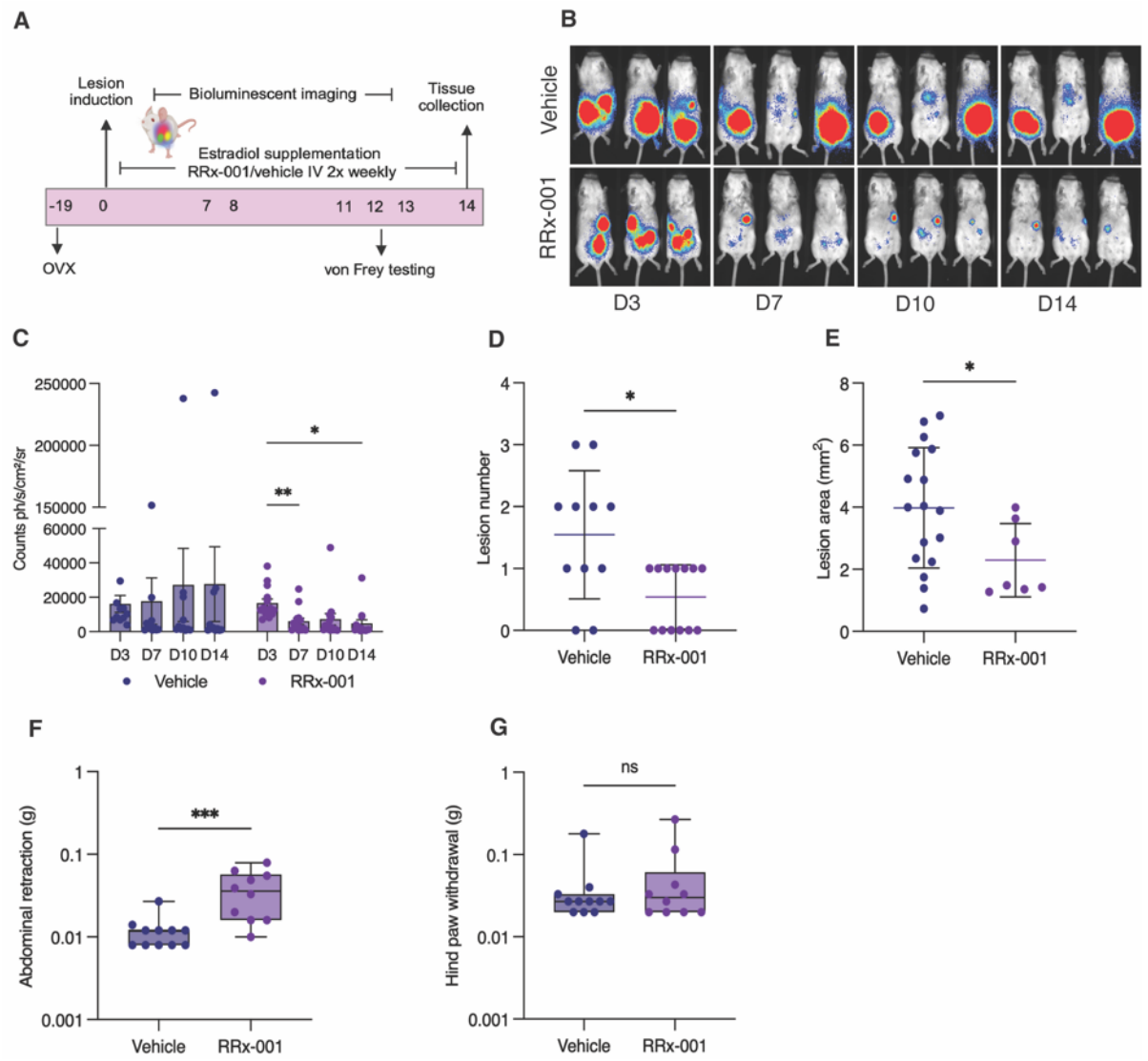

643

644 **Figure 1. RRx-001 reduces lesion growth and mechanical allodynia in a 'menses' model of induced**
645 **endometriosis**. (A) Schematic of experimental design. (B) Representative frontal images from days 3,
646 7, 10 and 14 from RRx-001 and vehicle treated mice. (C) Lesion bioluminescent signal of RRx-001 and
647 vehicle treated mice with endometriosis; statistical analysis performed using a two-way ANOVA with
648 Bonferroni post hoc. (D) Number of lesions and (E) size of lesions recovered from RRx-001 and vehicle
649 mice; statistical analyses performed using a Mann-Whitney test. (F) Mechanical hyperalgesia
650 measured using von Frey filaments applied to the abdomen and (G) hind paw (F and G plotted as an
651 average of 3 measurements taken over days 11-13 post-endometriosis induction; statistical analyses
652 performed using a Mann-Whitney test). * $p < 0.05$, ** $p < 0.01$, **** $p < 0.001$.

653

654

655

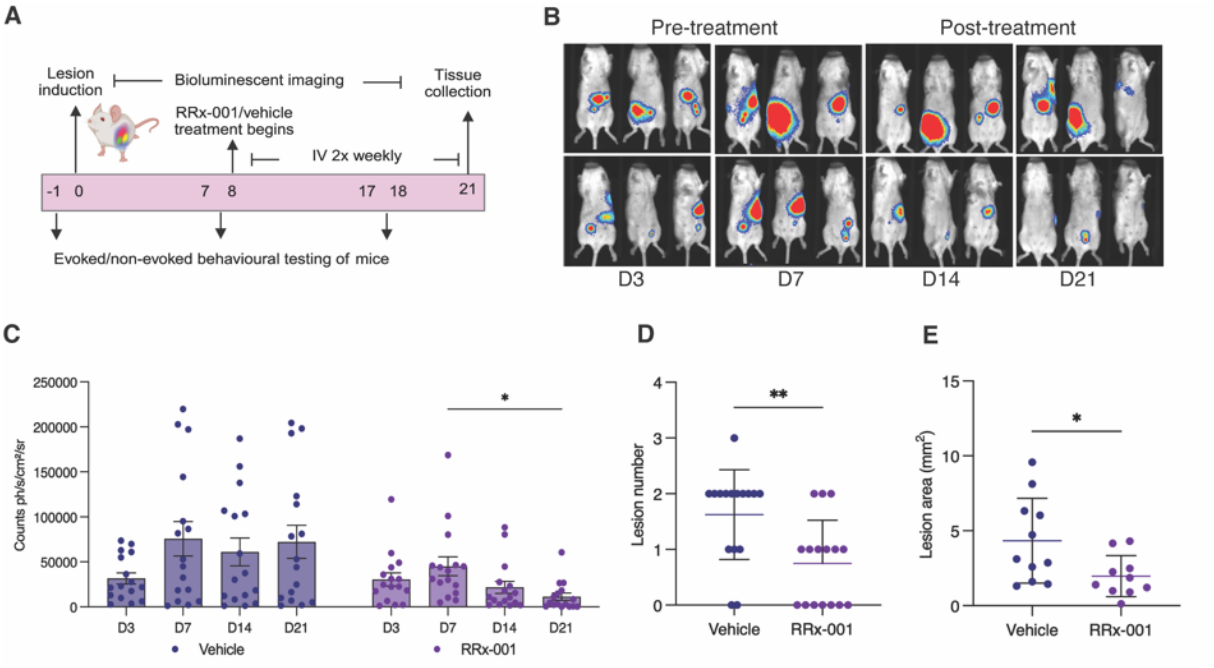

Figure 2. The impact of RRx-001 on lesion growth in a minimally invasive model of induced endometriosis. (A) Schematic of experimental design. (B) Representative frontal images from days 3, 7, 14 and 21 from RRx-001 and vehicle treated mice. (C) Bioluminescent signal of RRx-001 and vehicle treated mice; statistical analysis performed using a two-way ANOVA with Bonferroni post hoc. (D) Number of lesions and (E) size of lesions recovered from RRx-001 and vehicle mice; statistical analyses performed using a Mann-Whitney test. * $p < 0.05$, ** $p < 0.01$.

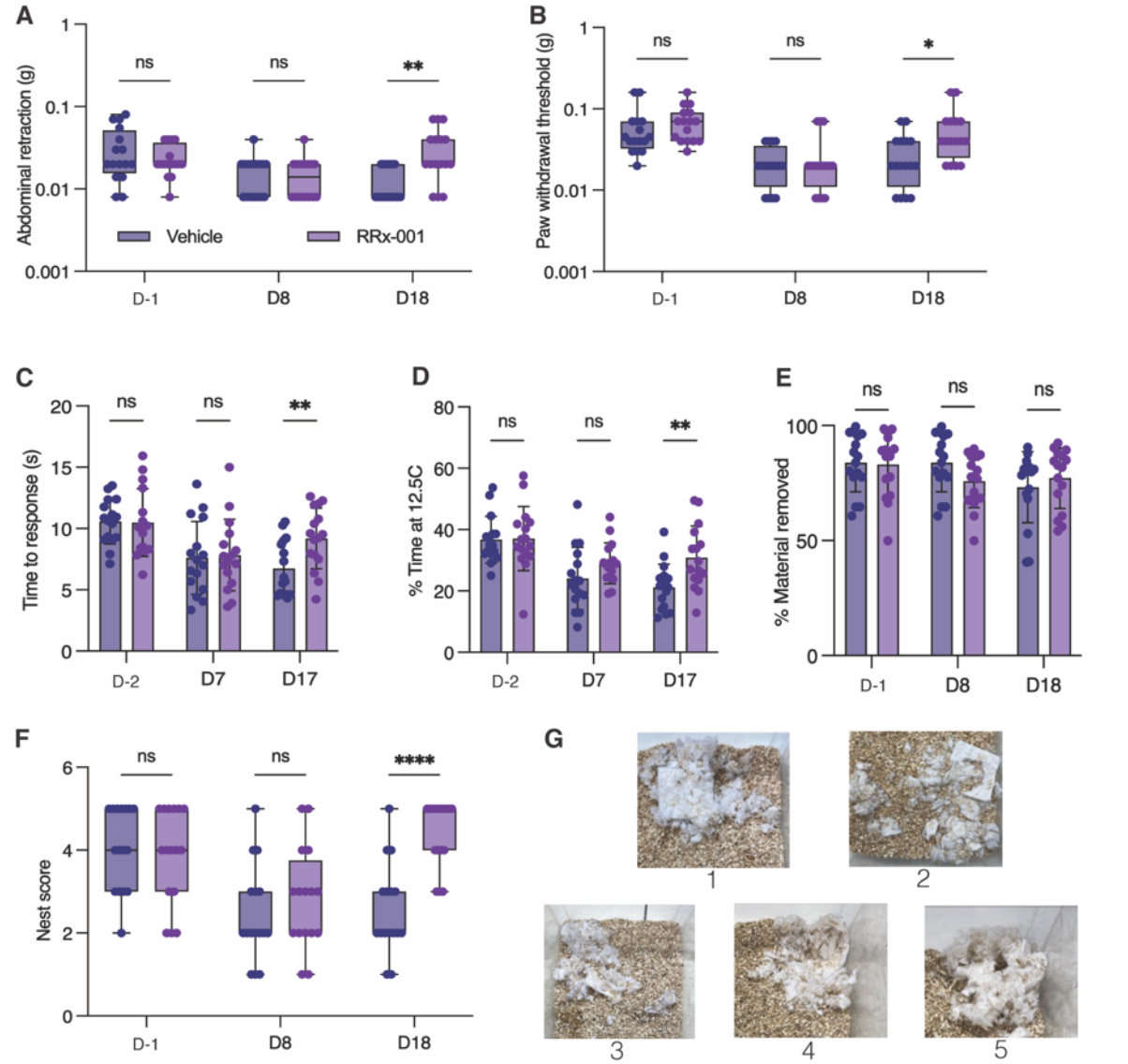

Figure 3. RRx-001 reduces evoked and non-evoked pain-associated behaviors in a minimally invasive model of induced endometriosis. (A) Mechanical allodynia measured using von Frey filaments applied to the abdomen and (B) hind paw; statistical analyses performed using multiple Mann-Whitney tests. (C) Hot plate latency assessed at 52°C; statistical analyses performed using multiple unpaired t-tests. (D) Percentage of material displaced in a burrowing assay; statistical analyses performed using multiple unpaired t-tests. (E) Thermal plate preference test analysis of % time spent on the 12.5 °C plate; statistical analyses performed using multiple unpaired t-tests. (F) Nest complexity scores; statistical analyses performed using multiple unpaired t-tests. (G) Example nests corresponding to scores 1-5. * $p < 0.05$, ** $p < 0.01$, **** $p < 0.0001$.

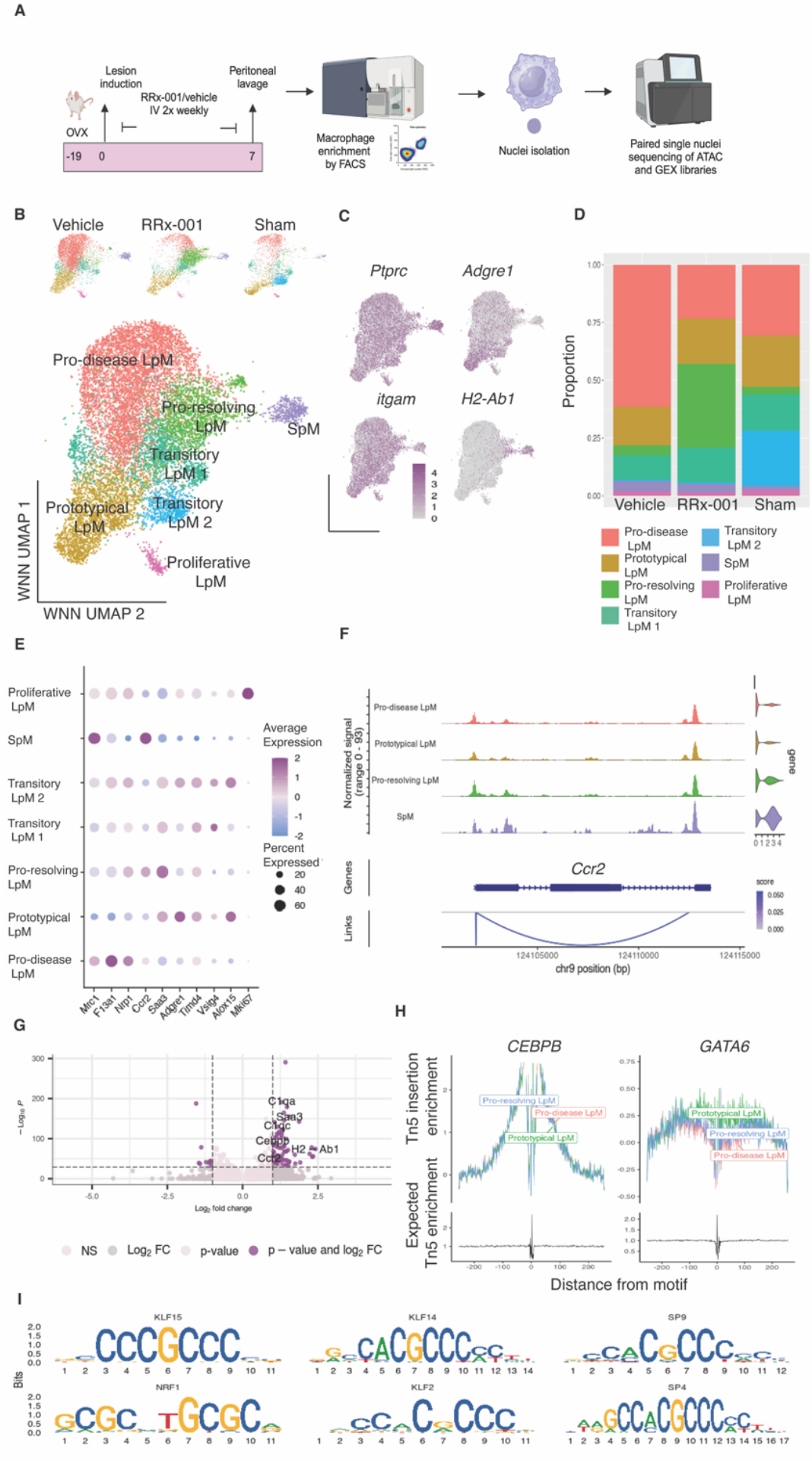
A
Lesion induction
Peritoneal lavage
RRx-001/vehicle IV 2x weekly
OVX
-19
0
7
Macrophage enrichment by FACS
Nuclei isolation
Paired single nuclei sequencing of ATAC and GEX libraries
B
Vehicle
RRx-001
Sham
Pro-disease LpM
Pro-resolving LpM
SpM
Transitory LpM 1
Prototypical LpM
Transitory LpM 2
Proliferative LpM
WNN UMAP 1
WNN UMAP 2
C
Ptprc
Adgre1
itgam
H2-Ab1
D
Proportion
Vehicle
RRx-001
Sham
Pro-disease LpM
Prototypical LpM
Pro-resolving LpM
Transitory LpM 1
Transitory LpM 2
SpM
Proliferative LpM
E
Proliferative LpM
SpM
Transitory LpM 2
Transitory LpM 1
Pro-resolving LpM
Prototypical LpM
Pro-disease LpM
Mrc1
F13a1
Nrp1
Ccr2
Saa3
Adgre1
Timd4
Vsig4
Alox15
Mki67
Average Expression
Percent Expressed
F
Normalized signal (range 0 - 93)
Pro-disease LpM
Prototypical LpM
Pro-resolving LpM
SpM
gene
Genes
Ccr2
Links
score
chr9 position (bp)
G
NS
Log2 FC
p-value
p – value and log2 FC
Log2 fold change
H
CEBPB
GATA6
Tn5 insertion enrichment
Expected Tn5 enrichment
Pro-resolving LpM
Pro-disease LpM
Prototypical LpM
Distance from motif
I
KLF15
KLF14
SP9
NRF1
KLF2
SP4
Bits

685

686 **Figure 4. Multiomic analyses of RNA and ATAC modalities of peritoneal macrophages.** (A) Schematic
687 of experimental design. (B) UMAP visualisation based on a weighted combination of RNA and ATAC
688 data from peritoneal macrophages isolated from vehicle treated endometriosis mice, RRx-001 treated
689 endometriosis mice and sham mice. Inset is UMAP projection split by sample ID. (C) Feature plots of
690 *Ptprc* (Cd45), *Itgam* (Cd11b), *Adgre1* (F4/80) and *H2-Ab1* (MhcII) expression levels. (D) Proportion of
691 each cluster occupied by each sample. (E) Dot plot of featured genes. (F) Chromatin accessibility, gene
692 expression data and peak-gene links for Ccr2 expression in selected macrophage populations. (G)
693 Volcano plot of up- and down-regulated DEGs of pro-resolving LpM compared to pro-disease LpM. (H)
694 Transcription factor footprinting of Cebpb and Gata6 in pro-resolving LpM, pro-disease LpM and
695 prototypical LpM populations. (I) DNA sequence motif enrichment analysis of ATAC data in peritoneal
696 macrophages derived from RRx-001 treated endometriosis mice.

697
698
699
700
701
702
703
704
705
706
707
708
709
710
711
712
713
714
715
716
717

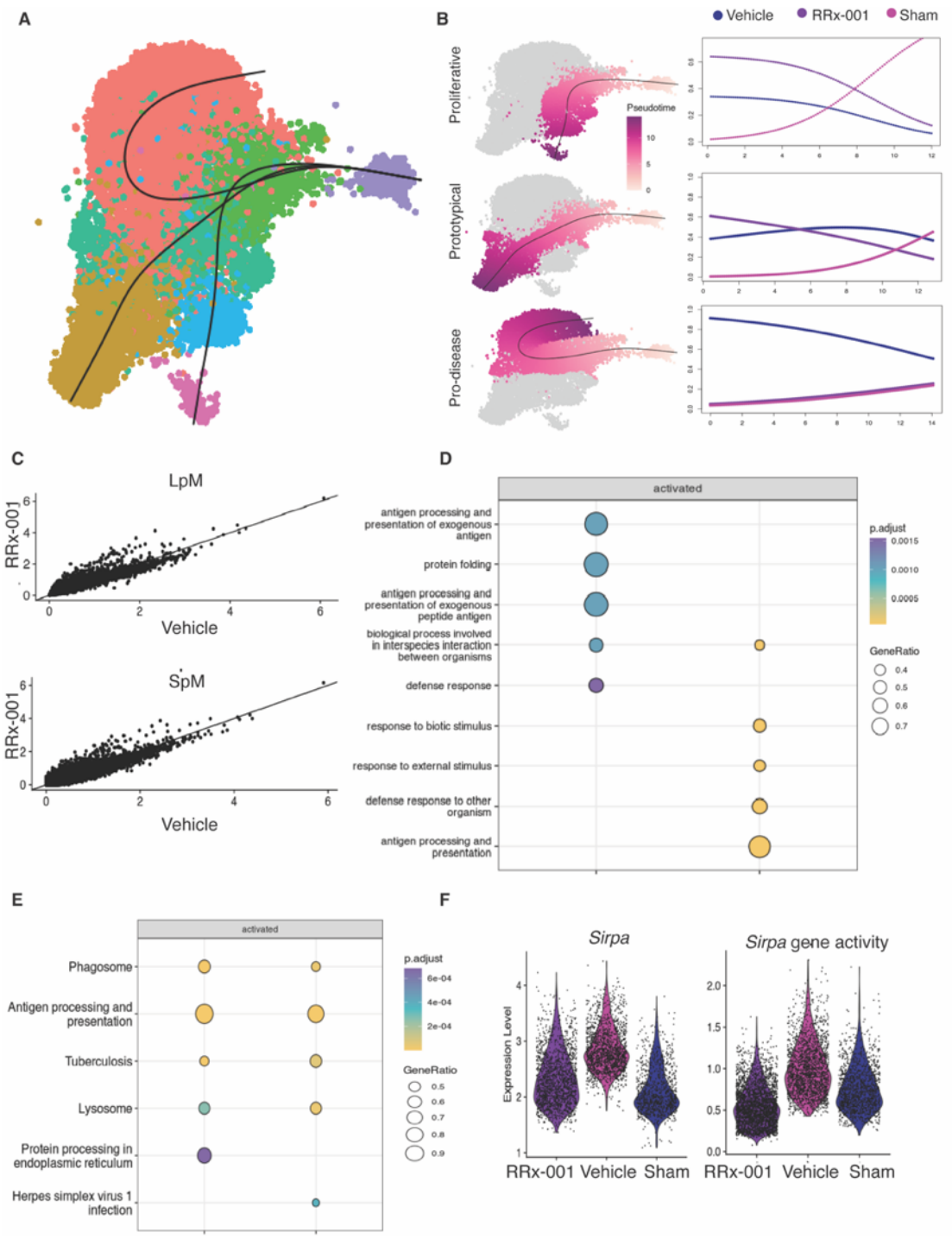

Figure 5. RRx-001 impacts differentiation trajectories and phenotypes of LpM and SpM populations in mice with induced endometriosis. (A) Slingshot fitted trajectories and principal curves. (B) Pseudotime ordering of inferred lineages (left) with multinomial logistic regression analysis of pseudo-temporal sample imbalance (right). (C) Scatter plot of aggregate (pseudobulk) expression of LpM and SpM populations from RRx-001 and vehicle treated mice (Pearson correlation reported). (D) ClusterProfiler gene set enrichment analysis using GO terms showing the top 5 terms in the LpM and SpM of RRx-001 treated mice with induced endometriosis. (E) ClusterProfiler gene set enrichment analysis using KEGG pathways showing the top 5 pathways in the LpM and SpM of RRx-001 treated

727 mice with induced endometriosis. (F) Violin plots of *Sirp*α expression in RNA-seq data and the gene
728 activity matrix derived from ATAC-seq data.

729
730
731
732
733
734
735
736
737
738
739
740
741
742
743
744
745
746
747
748
749
750
751
752
753
754
755
756
757

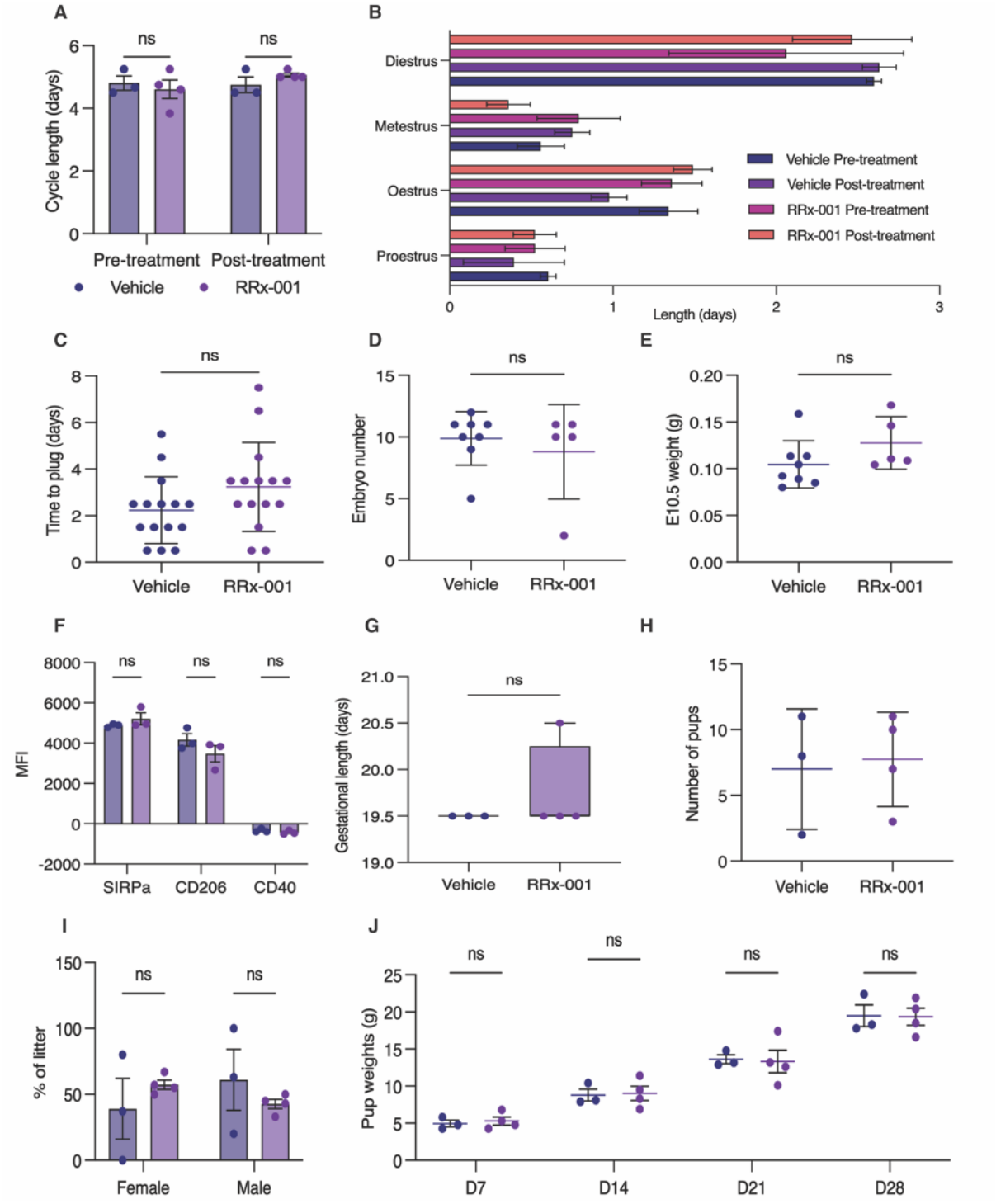

Figure 6. Pre-pregnancy treatment with RRx-001 does not cause oestrous cycle perturbations or impact reproductive function. (A) Length of oestrous cycle and (B) days spent within each stage; n=3 vehicle, n=4 RRx-001; statistical analyses performed using Student's t test and two-way ANOVA with Bonferroni post hoc. (C) Time to detection of seminal plug; n=15 RRx-001, n=15 vehicle; statistical analysis performed using a Student's t test. (D) Embryonic number and (E) average weight at E10.5; n=5 RRx-001, n=8 vehicle; statistical analyses performed using a Student's t test. (F) Median fluorescence intensity of SIRPα, CD206 (pro-repair) and CD40 (pro-inflammatory) in Hofbauer cells

766 pooled from 3 placentas per mouse at embryonic day 15.5; n=3 RRx-001, n=4 vehicle, statistical
767 analysis performed using Student's t test. (G) Gestational length of pregnancy, (H) number of pups
768 born to each mouse, (I) sex ratio of litter and (J) average litter weights from postnatal day 7 to
769 postnatal day 28; n=4 RRx-001, n=3 vehicle; statistical analyses performed using Student's t tests. No
770 statistical significance reached $p < 0.05$.

771
772
773
774
775
776
777
778
779
780
781
782
783
784
785
786
787
788
789
790
791
792
793
794
795
796
797
798
799

References

1. A. L. Shafrir, L. Farland, D. Shah, H. Harris, M. Kvaskoff, K. Zondervan, S. Missmer, Risk for and consequences of endometriosis: a critical epidemiologic review. *Best practice & research Clinical obstetrics & gynaecology* **51**, 1-15 (2018).
2. K. T. Zondervan, C. M. Becker, K. Koga, S. A. Missmer, R. N. Taylor, P. Viganò, Endometriosis. *Nature Reviews Disease Primers* **4**, 9 (2018).
3. T. Hirata, K. Koga, Y. Osuga, Extra-pelvic endometriosis: a review. *Reproductive medicine and biology* **19**, 323-333 (2020).
4. K. T. Zondervan, C. M. Becker, S. A. Missmer, Endometriosis. *N Engl J Med* **382**, 1244-1256 (2020).
5. K. Ellis, D. Munro, J. Clarke, Endometriosis is undervalued: a call to action. *Frontiers in Global Women's Health* **3**, 54 (2022).
6. J. A. Sampson, Metastatic or embolic endometriosis, due to the menstrual dissemination of endometrial tissue into the venous circulation. *The American journal of pathology* **3**, 93 (1927).
7. J. Halme, M. G. Hammond, J. F. Hulka, S. G. Raj, L. M. Talbert, Retrograde menstruation in healthy women and in patients with endometriosis. *Obstetrics and gynecology* **64**, 151-154 (1984).
8. L. K. Symons, J. E. Miller, V. R. Kay, R. M. Marks, K. Liblik, M. Koti, C. Tayade, The immunopathophysiology of endometriosis. *Trends in molecular medicine* **24**, 748-762 (2018).
9. A. W. Horne, S. A. Missmer, Pathophysiology, diagnosis, and management of endometriosis. *bmj* **379**, (2022).
10. R. O. Burney, L. C. Giudice, Pathogenesis and pathophysiology of endometriosis. *Fertility and sterility* **98**, 511-519 (2012).
11. M. H. Wu, K. Y. Hsiao, S. J. Tsai, Hypoxia: The force of endometriosis. *Journal of Obstetrics and Gynaecology Research* **45**, 532-541 (2019).
12. C. Chapron, L. Marcellin, B. Borghese, P. Santulli, Rethinking mechanisms, diagnosis and management of endometriosis. *Nature Reviews Endocrinology* **15**, 666-682 (2019).
13. K. Nirgianakis, L. Ma, B. McKinnon, M. D. Mueller, Recurrence patterns after surgery in patients with different endometriosis subtypes: a long-term hospital-based cohort study. *Journal of clinical medicine* **9**, 496 (2020).
14. G. Dunselman, N. Vermeulen, C. Becker, C. Calhaz-Jorge, T. D'Hooghe, B. De Bie, O. Heikinheimo, A. Horne, L. Kiesel, A. Nap, ESHRE guideline: management of women with endometriosis. *Human reproduction* **29**, 400-412 (2014).
15. C. M. Becker, W. T. Gattrell, K. Gude, S. S. Singh, Reevaluating response and failure of medical treatment of endometriosis: a systematic review. *Fertility and sterility* **108**, 125-136 (2017).
16. C. Hogg, A. W. Horne, E. Greaves, Endometriosis-associated macrophages: origin, phenotype, and function. *Frontiers in endocrinology* **11**, 7 (2020).
17. A. Shapouri-Moghaddam, S. Mohammadian, H. Vazini, M. Taghadosi, S. A. Esmaeili, F. Mardani, B. Seifi, A. Mohammadi, J. T. Afshari, A. Sahebkar, Macrophage plasticity, polarization, and function in health and disease. *J Cell Physiol* **233**, 6425-6440 (2018).
18. F. Ginhoux, M. Guilliams, Tissue-resident macrophage ontogeny and homeostasis. *Immunity* **44**, 439-449 (2016).
19. P. Italiani, D. Boraschi, From monocytes to M1/M2 macrophages: phenotypical vs. functional differentiation. *Frontiers in immunology* **5**, 514 (2014).

847 20. M. Bacci, A. Capobianco, A. Monno, L. Cottone, F. Di Puppo, B. Camisa, M. Mariani, C.
848 Brignole, M. Ponzoni, S. Ferrari, P. Panina-Bordignon, A. A. Manfredi, P. Rovere-Querini,
849 Macrophages are alternatively activated in patients with endometriosis and required for
850 growth and vascularization of lesions in a mouse model of disease. *Am J Pathol* **175**, 547-
851 556 (2009).
852 21. R. Forster, A. Sarginson, A. Velichkova, C. Hogg, A. Dorning, A. W. Horne, P. T. K.
853 Saunders, E. Greaves, Macrophage-derived insulin-like growth factor-1 is a key
854 neurotrophic and nerve-sensitizing factor in pain associated with endometriosis. *Faseb j* **33**,
855 11210-11222 (2019).
856 22. T. N. Ramírez-Pavez, M. Martínez-Esparza, A. J. Ruiz-Alcaraz, P. Marín-Sánchez, F.
857 Machado-Linde, P. García-Peñarrubia, The role of peritoneal macrophages in
858 endometriosis. *International Journal of Molecular Sciences* **22**, 10792 (2021).
859 23. C. C. Bain, C. A. Hawley, H. Garner, C. L. Scott, A. Schridde, N. J. Steers, M. Mack, A.
860 Joshi, M. Guilliams, A. M. I. Mowat, Long-lived self-renewing bone marrow-derived
861 macrophages displace embryo-derived cells to inhabit adult serous cavities. *Nature*
862 *communications* **7**, ncomms11852 (2016).
863 24. Y. Tan, W. F. Flynn, S. Sivajothi, D. Luo, S. B. Bozal, M. Davé, A. A. Luciano, P. Robson,
864 D. E. Luciano, E. T. Courtois, Single-cell analysis of endometriosis reveals a coordinated
865 transcriptional programme driving immunotolerance and angiogenesis across eutopic and
866 ectopic tissues. *Nat Cell Biol* **24**, 1306-1318 (2022).
867 25. M. Guo, C. Bafligil, T. Tapmeier, C. Hubbard, S. Manek, C. Shang, F. O. Martinez, N.
868 Schmidt, M. Obendorf, H. Hess-Stumpp, T. M. Zollner, S. Kennedy, C. M. Becker, K. T.
869 Zondervan, A. P. Cribbs, U. Oppermann, Mass cytometry analysis reveals a distinct immune
870 environment in peritoneal fluid in endometriosis: a characterisation study. *BMC Med* **18**, 3
871 (2020).
872 26. Y. Henlon, K. Panir, I. McIntyre, C. Hogg, P. Dhami, A. O. Cuff, A. Senior, N.
873 Moolchandani-Adwani, E. T. Courtois, A. W. Horne, M. Rosser, S. Ott, E. Greaves, Single-cell
874 analysis identifies distinct macrophage phenotypes associated with pro-disease and pro-
875 resolving functions in the endometriotic niche. *bioRxiv*, 2024.2003.2007.583861 (2024).
876 27. G. Zou, J. Wang, X. Xu, P. Xu, L. Zhu, Q. Yu, Y. Peng, X. Guo, T. Li, X. Zhang, Cell subtypes
877 and immune dysfunction in peritoneal fluid of endometriosis revealed by single-cell RNA-
878 sequencing. *Cell Biosci* **11**, 98 (2021).
879 28. J. Li, S. Yan, Q. Li, Y. Huang, M. Ji, X. Jiao, M. Yuan, G. Wang, Macrophage-associated
880 immune checkpoint CD47 blocking ameliorates endometriosis. *Mol Hum Reprod* **28**,
881 (2022).
882 29. C. Hogg, K. Panir, P. Dhami, M. Rosser, M. Mack, D. Soong, J. W. Pollard, S. J. Jenkins,
883 A. W. Horne, E. Greaves, Macrophages inhibit and enhance endometriosis depending on
884 their origin. *Proc Natl Acad Sci U S A* **118**, (2021).
885 30. J. Vallvé-Juanico, A. F. George, S. Sen, R. Thomas, M.-G. Shin, D. Kushnoor, J. J.
886 Vásquez, K. C. Vo, J. C. Irwin, N. R. Roan, Deep immunophenotyping reveals endometriosis
887 is marked by dysregulation of the mononuclear phagocytic system in endometrium and
888 peripheral blood. *BMC medicine* **20**, 1-19 (2022).
889 31. A. Labani-Motlagh, M. Ashja-Mahdavi, A. Loskog, The tumor microenvironment: a
890 milieu hindering and obstructing antitumor immune responses. *Frontiers in immunology*
891 **11**, 940 (2020).
892 32. K. Movahedi, D. Laoui, C. Gysemans, M. Baeten, G. Stangé, J. Van den Bossche, M.
893 Mack, D. Pipeleers, P. In't Veld, P. De Baetselier, Different tumor microenvironments

894 contain functionally distinct subsets of macrophages derived from Ly6C (high) monocytes.
895 *Cancer research* **70**, 5728-5739 (2010).
896 33. E. Azizi, A. J. Carr, G. Plitas, A. E. Cornish, C. Konopacki, S. Prabhakaran, J. Nainys, K.
897 Wu, V. Kiseliovas, M. Setty, Single-cell map of diverse immune phenotypes in the breast
898 tumor microenvironment. *Cell* **174**, 1293-1308. e1236 (2018).
899 34. Y. Pan, Y. Yu, X. Wang, T. Zhang, Tumor-associated macrophages in tumor immunity.
900 *Frontiers in immunology* **11**, 583084 (2020).
901 35. A. Mantovani, F. Marchesi, A. Malesci, L. Laghi, P. Allavena, Tumour-associated
902 macrophages as treatment targets in oncology. *Nature reviews Clinical oncology* **14**, 399-
903 416 (2017).
904 36. A. Mantovani, P. Allavena, F. Marchesi, C. Garlanda, Macrophages as tools and targets
905 in cancer therapy. *Nature Reviews Drug Discovery* **21**, 799-820 (2022).
906 37. N. Jayabalan, B. Oronsky, P. Cabrales, T. Reid, S. Caroen, A. M. Johnson, N. A. Birch, J.
907 D. O'Sullivan, R. Gordon, A review of RRx-001: a late-stage multi-indication inhibitor of
908 NLRP3 activation and chronic inflammation. *Drugs* **83**, 389-402 (2023).
909 38. A. Dorning, P. Dhami, K. Panir, C. Hogg, E. Park, G. D. Ferguson, D. Hargrove, J. Karras,
910 A. W. Horne, E. Greaves, Bioluminescent imaging in induced mouse models of
911 endometriosis reveals differences in four model variations. *Dis Model Mech* **14**, (2021).
912 39. B. Oronsky, C. A. Carter, S. Caroen, C. Scribner, A. Oronsky, T. R. Reid, RRx-001, a first-
913 in-class small molecule inhibitor of MYC and a downregulator of CD47, is an"
914 erythrophagoimmunotherapeutic". *OncoImmunology* **9**, 1746172 (2020).
915 40. M. A. Tejada, C. Antunez, P. Nunez-Badinez, B. De Leo, P. T. Saunders, K. Vincent, A.
916 Cano, J. Nagel, R. Gomez, Rodent Animal Models of Endometriosis-Associated Pain: Unmet
917 Needs and Resources Available for Improving Translational Research in Endometriosis.
918 *International Journal of Molecular Sciences* **24**, 2422 (2023).
919 41. Y. Hao, S. Hao, E. Andersen-Nissen, W. M. Mauck, S. Zheng, A. Butler, M. J. Lee, A. J.
920 Wilk, C. Darby, M. Zager, Integrated analysis of multimodal single-cell data. *Cell* **184**, 3573-
921 3587. e3529 (2021).
922 42. L. Zhao, M. Shi, S. Winuthayanon, J. A. MacLean, K. Hayashi, Niclosamide targets the
923 dynamic progression of macrophages for the resolution of endometriosis in a mouse model.
924 *Communications Biology* **5**, 1225 (2022).
925 43. P. A. Louwe, L. Badiola Gomez, H. Webster, G. Perona-Wright, C. C. Bain, S. J. Forbes,
926 S. J. Jenkins, Recruited macrophages that colonize the post-inflammatory peritoneal niche
927 convert into functionally divergent resident cells. *Nat Commun* **12**, 1770 (2021).
928 44. D. Dörr, B. Obermayer, J. M. Weiner, K. Zimmermann, C. Anania, L. K. Wagner, E. M.
929 Lyras, V. Sapozhnikova, D. Lara-Astiaso, F. Prósper, C/EBPβ regulates lipid metabolism and
930 Pparg isoform 2 expression in alveolar macrophages. *Science Immunology* **7**, eabj0140
931 (2022).
932 45. M. Rosas, L. C. Davies, P. J. Giles, C.-T. Liao, B. Kharfan, T. C. Stone, V. B. O'Donnell, D.
933 J. Fraser, S. A. Jones, P. R. Taylor, The transcription factor Gata6 links tissue macrophage
934 phenotype and proliferative renewal. *Science* **344**, 645-648 (2014).
935 46. Y. Yuan, G. Fan, Y. Liu, L. Liu, T. Zhang, P. Liu, Q. Tu, X. Zhang, S. Luo, L. Yao, F. Chen, J.
936 Li, The transcription factor KLF14 regulates macrophage glycolysis and immune function by
937 inhibiting HK2 in sepsis. *Cellular & Molecular Immunology* **19**, 504-515 (2022).
938 47. B. Oronsky, L. Takahashi, R. Gordon, P. Cabrales, S. Caroen, T. Reid, RRx-001: a
939 chimeric triple action NLRP3 inhibitor, Nrf2 inducer, and nitric oxide superagonist. *Front*
940 *Oncol* **13**, 1204143 (2023).

941 48. L. Van Putten, F. Croon, The life span of red cells in the rat and the mouse as
942 determined by labeling with DFP32 in vivo. *Blood* **13**, 789-794 (1958).
943 49. L. Zhang, W. Long, W. Xu, X. Chen, X. Zhao, B. Wu, Digital cell atlas of mouse uterus:
944 from regenerative stage to maturational stage. *Frontiers in Genetics* **13**, 847646 (2022).
945 50. W. K. Whitten, Modification of the oestrous cycle of the mouse by external stimuli
946 associated with the male. *Journal of Endocrinology* **13**, 399-404 (1956).
947 51. L. Reyes, B. Wolfe, T. Golos, Hofbauer cells: placental macrophages of fetal origin.
948 *Macrophages: origin, functions and biointervention*, 45-60 (2017).
949 52. C. A. Carter, B. Schmitz, P. G. Peterson, M. Quinn, A. Degesys, J. Jenkins, B. Oronsky, J.
950 Scicinski, S. Caroen, T. R. Reid, Immune reactivity and pseudoprogression or tumor flare in
951 a serially biopsied neuroendocrine patient treated with the epigenetic agent RRx-001. *Case*
952 *reports in oncology* **9**, 164-170 (2016).
953 53. R. M. Deacon, Assessing nest building in mice. *Nat Protoc* **1**, 1117-1119 (2006).
954 54. H. Zhao, S. Ning, J. Scicinski, B. Oronsky, S. J. Knox, D. M. Peehl, Epigenetic effects of
955 RRx-001: a possible unifying mechanism of anticancer activity. *Oncotarget* **6**, 43172-43181
956 (2015).
957 55. T. Reid, B. Oronsky, J. Scicinski, C. L. Scribner, S. J. Knox, S. Ning, D. M. Peehl, R. Korn,
958 M. Stirn, C. A. Carter, A. Oronsky, M. J. Taylor, W. L. Fitch, P. Cabrales, M. M. Kim, H. A.
959 Burris, C. D. Lao, N. E. D. Abrouk, G. R. Fanger, J. R. Infante, Safety and activity of RRx-001
960 in patients with advanced cancer: a first-in-human, open-label, dose-escalation phase 1
961 study. *The Lancet Oncology* **16**, 1133-1142 (2015).
962 56. M. H. Fens, P. Cabrales, J. Scicinski, S. K. Larkin, J. H. Suh, F. A. Kuypers, N. Oronsky, M.
963 Lybeck, A. Oronsky, B. Oronsky, Targeting tumor hypoxia with the epigenetic anticancer
964 agent, RRx-001: a superagonist of nitric oxide generation. *Med Oncol* **33**, 85 (2016).
965 57. B. Oronsky, P. Cabrales, S. Caroen, X. Guo, C. Scribner, A. Oronsky, T. R. Reid, RRx-001,
966 a downregulator of the CD47- SIRPα checkpoint pathway, does not cause anemia or
967 thrombocytopenia. *Expert Opin Drug Metab Toxicol* **17**, 355-357 (2021).
968 58. P. Cabrales, RRx-001 Acts as a Dual Small Molecule Checkpoint Inhibitor by
969 Downregulating CD47 on Cancer Cells and SIRP-α on Monocytes/Macrophages. *Transl*
970 *Oncol* **12**, 626-632 (2019).
971 59. H. Zhao, S. Ning, R. Nolley, J. Scicinski, B. Oronsky, S. J. Knox, D. M. Peehl, The
972 immunomodulatory anticancer agent, RRx-001, induces an interferon response through
973 epigenetic induction of viral mimicry. *Clin Epigenetics* **9**, 4 (2017).
974 60. E. Greaves, F. L. Cousins, A. Murray, A. Esnal-Zufiaurre, A. Fassbender, A. W. Horne, P.
975 T. Saunders, A novel mouse model of endometriosis mimics human phenotype and reveals
976 insights into the inflammatory contribution of shed endometrium. *Am J Pathol* **184**, 1930-
977 1939 (2014).
978 61. A. C. McLean, N. Valenzuela, S. Fai, S. A. Bennett, Performing vaginal lavage, crystal
979 violet staining, and vaginal cytological evaluation for mouse estrous cycle staging
980 identification. *J Vis Exp*, e4389 (2012).
981 62. E. Greaves, A. W. Horne, H. Jerina, M. Mikolajczak, L. Hilferty, R. Mitchell, S. M.
982 Fleetwood-Walker, P. T. Saunders, EP2 receptor antagonism reduces peripheral and central
983 hyperalgesia in a preclinical mouse model of endometriosis. *Sci Rep* **7**, 44169 (2017).
984 63. K. Ottersbach, E. Dzierzak, in *Leukemia: Methods and Protocols,* C. W. Eric So, Ed.
985 (Humana Press, Totowa, NJ, 2009), pp. 335-346.
986 64. G. Liang, B. Huang, F. Wang, F. Liu, Protocols for isolation and characterization of
987 mouse placental hemogenic endothelial cells. *STAR protocols* **2**, 100884 (2021).

65. L. Heumos, A. C. Schaar, C. Lance, A. Litinetskaya, F. Drost, L. Zappia, M. D. Lücken, D. C. Strobl, J. Henao, F. Curion, Best practices for single-cell analysis across modalities. *Nature Reviews Genetics* **24**, 550-572 (2023).
66. Y. Zhang, T. Liu, C. A. Meyer, J. Eeckhoute, D. S. Johnson, B. E. Bernstein, C. Nusbaum, R. M. Myers, M. Brown, W. Li, Model-based analysis of ChIP-Seq (MACS). *Genome biology* **9**, 1-9 (2008).
67. Y. Yoshimura, Y. Muto, N. Ledru, H. Wu, K. Omachi, J. H. Miner, B. D. Humphreys, A single-cell multiomic analysis of kidney organoid differentiation. *Proceedings of the National Academy of Sciences* **120**, e2219699120 (2023).
68. P.-L. Germain, A. Lun, C. G. Meixide, W. Macnair, M. D. Robinson, Doublet identification in single-cell sequencing data using scDblFinder. *F1000Research* **10**, (2021).
69. M. D. Young, S. Behjati, SoupX removes ambient RNA contamination from droplet-based single-cell RNA sequencing data. *Gigascience* **9**, giaa151 (2020).
70. I. Korsunsky, N. Millard, J. Fan, K. Slowikowski, F. Zhang, K. Wei, Y. Baglaenko, M. Brenner, P.-r. Loh, S. Raychaudhuri, Fast, sensitive and accurate integration of single-cell data with Harmony. *Nature methods* **16**, 1289-1296 (2019).
71. G. Finak, A. McDavid, M. Yajima, J. Deng, V. Gersuk, A. K. Shalek, C. K. Slichter, H. W. Miller, M. J. McElrath, M. Prlic, MAST: a flexible statistical framework for assessing transcriptional changes and characterizing heterogeneity in single-cell RNA sequencing data. *Genome biology* **16**, 1-13 (2015).
72. T. Stuart, A. Butler, P. Hoffman, C. Hafemeister, E. Papalexi, W. M. Mauck, Y. Hao, M. Stoeckius, P. Smibert, R. Satija, Comprehensive integration of single-cell data. *cell* **177**, 1888-1902. e1821 (2019).
73. K. Blighe, S. Rana, M. Lewis, EnhancedVolcano: Publication-ready volcano plots with enhanced colouring and labeling. *R package version* **1**, 10.18129 (2019).
74. T. Stuart, A. Srivastava, S. Madad, C. A. Lareau, R. Satija, Single-cell chromatin state analysis with Signac. *Nature Methods* **18**, 1333-1341 (2021).
75. G. Yu, L.-G. Wang, Y. Han, Q.-Y. He, clusterProfiler: an R package for comparing biological themes among gene clusters. *Omics: a journal of integrative biology* **16**, 284-287 (2012).
76. W. Saelens, R. Cannoodt, H. Todorov, Y. Saeys, A comparison of single-cell trajectory inference methods. *Nature biotechnology* **37**, 547-554 (2019).
77. K. Street, D. Risso, R. B. Fletcher, D. Das, J. Ngai, N. Yosef, E. Purdom, S. Dudoit, Slingshot: cell lineage and pseudotime inference for single-cell transcriptomics. *BMC genomics* **19**, 1-16 (2018).

1032 **Supplementary Figures**

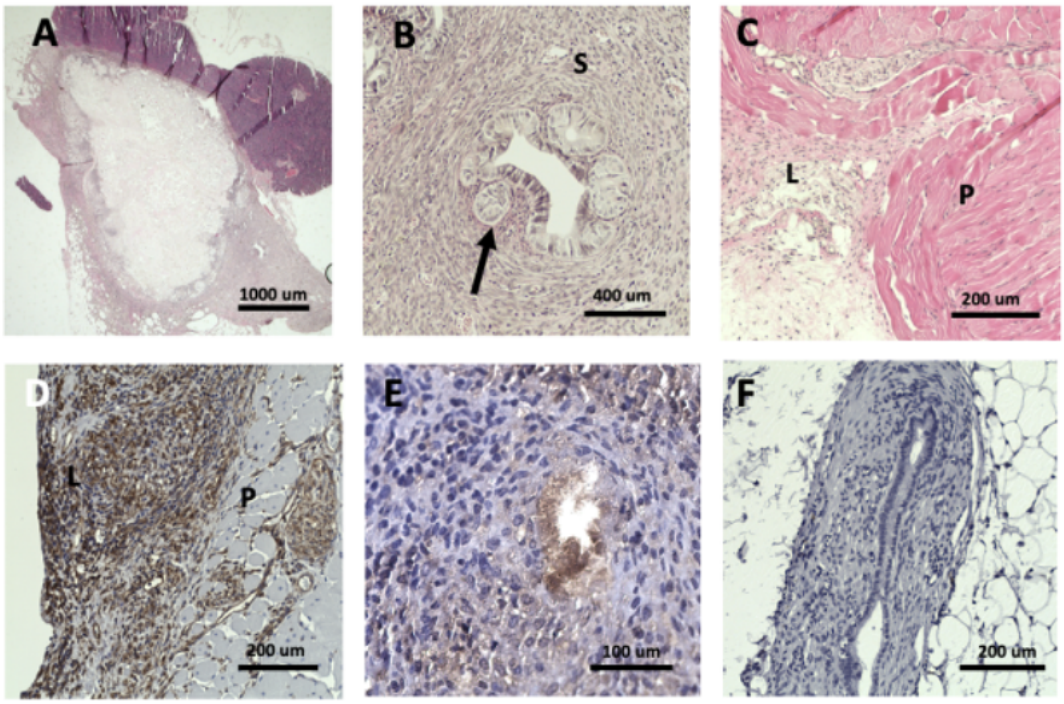

1033
1034 **Figure S1: Histological verification of lesions.** (A-C) Representative hematoxylin and eosin stains of
1035 recovered lesions. (A) Cystic lesion, (B) glandular (arrow) and stromal structures (S) within lesion. (C)
1036 Lesion (L) infiltration into the peritoneal wall (P). (D) Stromal (vimentin^{+} cells) on a peritoneal wall
1037 lesion. (E) Epithelial (cytokeratin^{+} cells) showing staining of a glandular structure. (F) Negative control.
1038 Scale bars as shown.
1039
1040
1041
1042
1043
1044
1045
1046
1047
1048
1049
1050
1051
1052
1053

1054

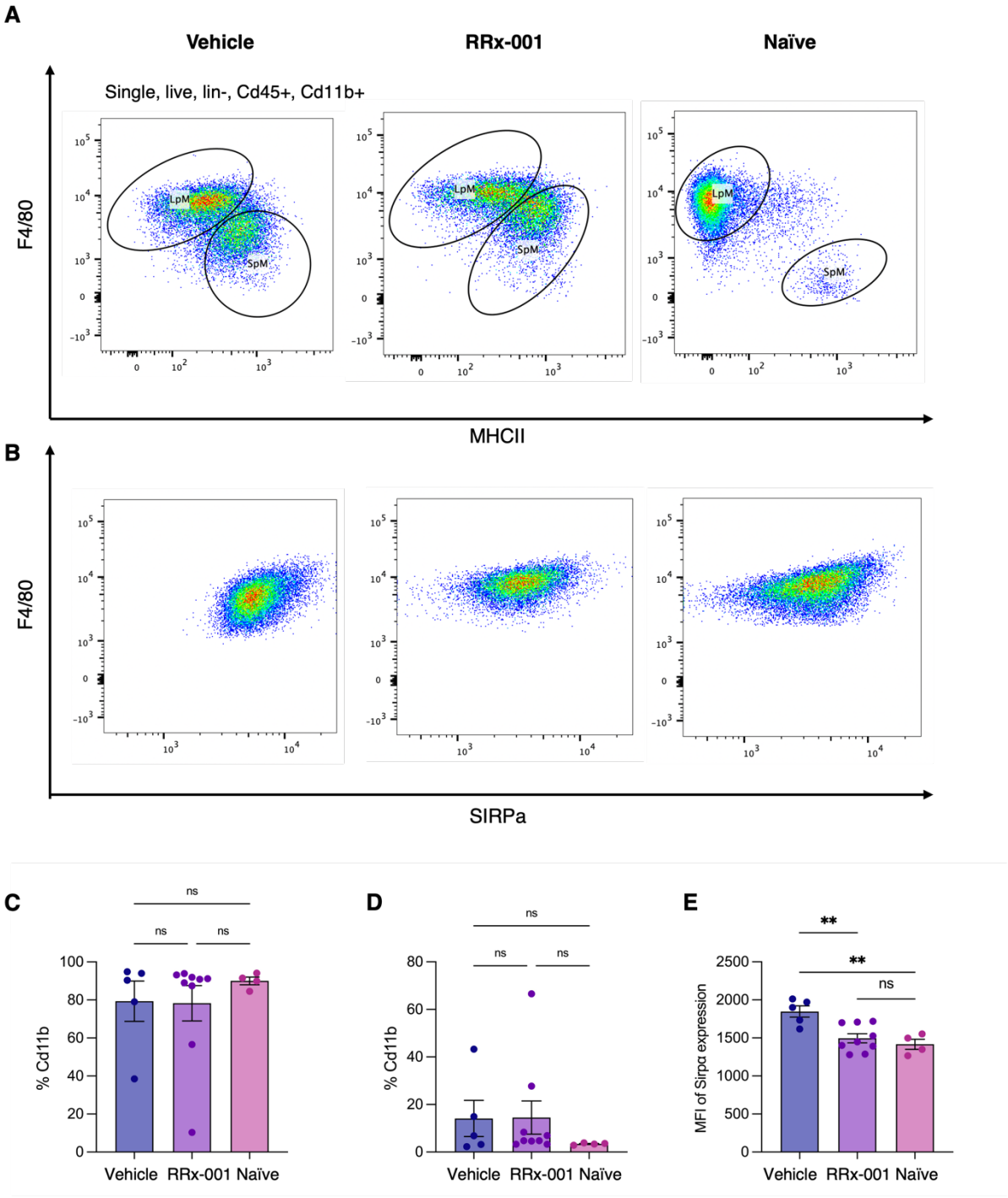

1055

1056

1057 **Figure S2: Representative flow plots of peritoneal macrophage sub-populations and expression of**

1058 **Sirpα.** (A) Representative flow plots of LpM and SpM populations in vehicle, RRx-001 treated and naïve

1059 mice. (B) LpM population and Sirpα expression. (C) Percentage of Cd11b+ cells that are LpM and (D)

1060 SpM. (E) Median fluorescence intensity of Sirpα on LpM.

1061

1062

1063

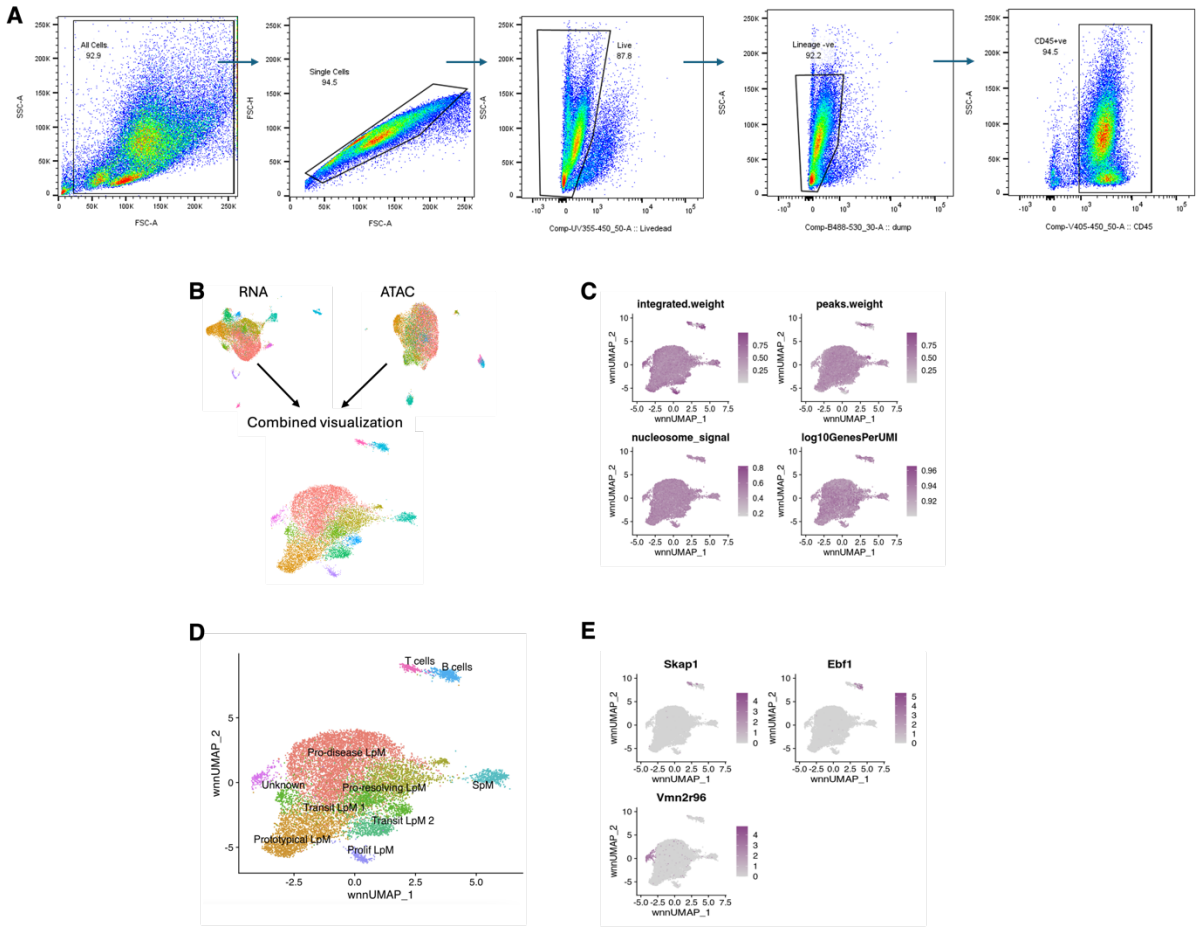

1064

1065 **Figure S3: Isolation of macrophage for integrative weighted nearest neighbours (WNN) analysis.** (A)
1066 Flow cytometry gating strategy. (B) UMAP visualisations of individual RNA and ATAC modalities and
1067 their integrated joint WNN visualisation. (C) RNA and ATAC modality weight across clusters,
1068 nucleosome signal (ATAC) and log10GenesPerUMI (RNA). (D) Clusters corresponding to T, B or
1069 unknown immune cells were removed by identification using marker genes shown in (E) Feature plots
1070 of Skap1, Ebf1 and Vmn2r96, respectively.

1071